

Visualizing mesoderm and neural crest cell dynamics during chick head morphogenesis

Mary Cathleen McKinney¹, Rebecca McLennan¹, Rasa Giniunaite², Ruth E. Baker²,
Philip K. Maini², Hans G. Othmer³, Paul M Kulesa^{1,4}

1. Stowers Institute for Medical Research, Kansas City, MO, 64110, USA
2. University of Oxford, Wolfson Centre for Mathematical Biology, Mathematical Institute, Woodstock Road, Oxford, OX2 6GG, UK
3. School of Mathematics, 270A Vincent Hall, University of Minnesota, Minneapolis, MN, 55455, USA
4. Department of Anatomy and Cell Biology, University of Kansas School of Medicine, Kansas City, KS, 66160, USA

*corresponding author: pmk@stowers.org

Highlights:

- Simultaneous time-lapse imaging of head mesoderm, ectoderm and neural crest cells
- Mesodermal cells move in a collective, directed manner but slower than neural crest
- Mesoderm grows non-uniform in space and time
- Neural crest and mesoderm cells communicate to regulate growth and migration
- Model simulations predict neural crest migration is robust to growth heterogeneity

Keywords: time-lapse, tissue growth, neural crest, mesoderm, avian, computer modeling

ABSTRACT

Vertebrate head morphogenesis involves carefully orchestrated tissue growth and cell movements of the mesoderm and neural crest to form the distinct craniofacial pattern. To better understand structural birth defects, it is important that we characterize the dynamics of these processes and learn how they rely on each other. Here we examine this question during chick head morphogenesis using time-lapse imaging, computational modeling, and experiments. We find that head mesodermal cells in culture move in random directions as individuals and move faster in the presence of neural crest cells. In vivo, mesodermal cells migrate in a directed manner and maintain neighbor relationships; neural crest cells travel through the mesoderm at a faster speed. The mesoderm grows with a non-uniform spatio-temporal profile determined by BrdU labeling during the period of faster and more directed neural crest collective migration through this domain. We use computer simulations to probe the robustness of neural crest stream formation by varying the spatio-temporal growth profile of the mesoderm. We follow this with experimental manipulations that either stop mesoderm growth or prevent neural crest migration and observe changes in the non-manipulated cell population, implying a dynamic feedback between tissue growth and neural crest cell signaling to confer robustness to the system. Overall, we present a novel descriptive analysis of mesoderm and neural crest cell dynamics that reveals the coordination and co-dependence of these two cell populations during head morphogenesis.

INTRODUCTION

Vertebrate head morphogenesis is a process that involves the rapid growth and dynamic behaviors of several cell populations to form the face, jaw, and branchial arches. These cell populations that include the ectoderm, mesoderm, and neural crest must be coordinated in a well-orchestrated choreography to produce the proper axial pattern of the head. For example, to reach the periphery after exiting the dorsal neural tube, cranial neural crest cells must travel through dense extracellular matrix and mesoderm, subjacent to the ectoderm (Tosney, 1982; Noden, 1988). Tissue transplantations, together with viral and fluorescent dye marking of the cranial neural crest and paraxial mesoderm have revealed that both cell types are migratory and follow stereotypical pathways into the branchial arches (Kontges and Lumsden, 1996; Hacker and Guthrie, 1998; Evans and Noden, 2006). However, these static analyses have not been able to tease out the cell dynamics and the relationship between cell proliferation, tissue growth and cell-cell interactions that contribute to the complexity of head morphogenesis. This is primarily due to the lack of a detailed *in vivo* analysis of head mesoderm and ectoderm dynamics in space and time, and limitations with *in vivo* imaging of neural crest-mesodermal cell interactions.

A better understanding of the dynamics and interplay between the neural crest and tissues through which these cells travel would shed light on the mechanistic basis of collective cell migration, for which neural crest cells are an exemplary model (reviewed in (Noden and Trainor, 2005; Kulesa and McLennan, 2015; Szabo and Mayor, 2016). Detailed experiments, together with mathematical modeling, provide a means to explore the robustness of the stereotypical cranial neural crest cell migratory pathways and distance migrated by cells during early head development under the constraints of a growing microenvironment. In the absence of dynamic data, it is possible to speculate on a wide variety of tissue growth profiles for the head mesoderm and their potential impact on collective neural crest cell migration. For example, in previous work, we quantified a curvilinear measurement of the distance from the chick neural tube dorsal midline along the dorsolateral cranial neural crest cell migratory pathway, to the tip of branchial arch 2 (ba2) throughout early developmental stages (McLennan et al., 2012;

McLennan et al., 2017). This simple length measurement revealed a logistic growth profile of the total neural crest cell migratory domain over time (McLennan et al., 2017), but left unanswered the question of whether there is non-uniform growth of the mesoderm in space.

In this study, we investigate the spatial and temporal dynamics of individual mesoderm and ectoderm cells, and their interplay with migrating neural crest cells during head morphogenesis. We examine and quantify the inherent migratory properties of mesoderm either isolated from or in the presence of neural crest cells, as a baseline for in vivo comparison. We then visualize and quantify head ectoderm, mesoderm and neural crest cell behaviors simultaneously in Tg(hUBC: H2BCerulean-2A-Dendra2) whole quail embryo explants. We image BrdU and methyl green nuclear labels in cleared whole chick embryos to distinguish proliferative subregions within the head mesoderm throughout successive chick developmental stages during neural crest cell migration. In addition, we computationally explore the impact of different spatially non-uniform mesoderm growth profiles and converge on a subset of possible outcomes that result in a continuous neural crest cell migratory stream. To address how changes in either the presence of neural crest cells or mesodermal cell proliferation affect cell dynamics and branchial arch size, we ablate a subregion of premigratory neural crest cells and measure subsequent tissue growth. Separately, we apply aphidicolin and hydroxyurea by focal microinjection into paraxial mesoderm to inhibit cell proliferation and compare the distribution of neural crest cells along the migratory domain with our computational model predictions. Together, our data offer the first detailed characterization of cell and tissue growth dynamics in the vertebrate head and how neural crest cells must respond to migrate in a collective and directed manner.

MATERIALS AND METHODS

Embryos and in ovo labeling

Fertilized white leghorn chicken (Centurion Poultry) or Tg(hUBC: H2BCerulean-2A-Dendra2) quail eggs (Translational Imaging Center, University of Southern California) were incubated at 38° C in a humidified incubator until the desired Hamburger and Hamilton (HH) stage (Hamburger and Hamilton, 1951) of development. A 0.3M sucrose solution was mixed 1:1 with DiD vibrant dye solution (V22887 Thermo Fisher) and injected into the neural tubes of embryos at HH9 for neural crest labeling.

In vitro assays

For mesoderm and neural tube cultures, glass bottomed petri dishes (P35G-1.5-20C, Mattek) were coated with 20ug/ml of fibronectin (F1141; Millipore Sigma) and 20ug/ml of poly-D-lysine (P7886; Millipore Sigma) for 30 minutes before being allowed to dry. Lateral mesoderm tissue from the r4 axial level was isolated from stage HH6-8 chick embryos by creating transverse cuts at the r3/r4 and r4/r5 borders and then removing neural tube, ectoderm and endoderm with a sharpened tungsten needle and forceps. The remaining mesoderm was placed onto prepared glass bottomed dishes. Isolated neural tube explants were prepared similarly to (McLennan et al., 2010) and placed in a separate dish or near the mesoderm tissue. Cells were cultured in Ham's F-12 nutrient mix (11765047; Thermo Fisher) supplemented with Pen/Strep and B27 (17504044, Thermo Fisher) at 37° either in a tissue culture incubator or in an environmental chamber on the microscope. For in vitro experiments with VEGF, 100ug/mL of VEGF (293-VE-010, R&D systems) was added to the F-12 media for 16-hour incubation or PBS for control. Cells were labeled with 5ug/mL of Hoechst 33342 (b2261, Millipore Sigma) for 10 minutes either for live imaging or after immunohistochemistry. Glass bottomed dishes for in vitro cultures were placed in a 6-well microscope stage insert inside a heated environmental chamber on an LSM-800 confocal microscope (Zeiss) and imaged every 5 minutes, using a Plan Apochromat 10x 0.45 NA M27 objective, single z plane, with a minimum of 405 laser intensity for 16 or more hours. Analysis was performed on many cells from multiple time lapses (three

mesoderm/neural tube, five mesoderm only, four neural tube only, three mesoderm and ectoderm). Significance was determined with a two-tailed Student's T-test throughout the manuscript.

Antibody labeling

For proliferation studies in vivo, the vitelline membrane was removed from the head of the embryo and then 50uL of BrdU labeling reagent (000103, Thermo Fisher) was dropped on top. The embryos were reincubated for 30 min then fixed in 4% paraformaldehyde overnight at 4°. The head and first four somites were isolated from the trunk and then embryos HH13 and older were bisected down the midline. For immunohistochemistry, fixed embryos were incubated for 10 minutes in 1N HCl on ice, 10 minutes in 2N HCl at room temperature followed by 20 minutes at 37°. After 12 minutes in Borate buffer, the embryos were incubated with PBS+1% TritonX and finally 10% goat serum (16210072, Thermo Fisher) block. In vitro cultures were prepared by adding 1% BrdU labeling reagent and cultured for 1 hour before fixing with 4% paraformaldehyde for 30 minutes at room temperature. In vitro protocols only require 15 minutes 1N HCl at 37° and 15' Borate buffer before washing and blocking. Embryos or cells were labeled with primary antibodies BrdU (1:200, pa5-32256, ThermoFisher, Lot TH2627941A) and HNK-1 (1:25, TIB-200, ATCC) in block overnight at 4°. After extensive washing in block at room temperature, secondary antibodies-goat anti-rabbit IgG Alexa Fluor 488 and goat anti-mouse IgM AlexaFluor 546 (A-11008 and A-21045, Thermo Fisher)-- were applied at a 1:500 dilution overnight at 4°. For a nuclear stain, Methyl Green (1:5000, M8884 Millipore Sigma, (Prieto et al., 2015)) was added to embryos after immunohistochemistry for several hours. Embryos with no primary antibody were used as control. Embryos were cleared for imaging using 80% FRUIT clearing buffer (Hou et al., 2015) overnight at 4° and mounted for imaging in 80% FRUIT buffer on glass slides. At least 3, and up to 5, embryos' data were combined for each stage.

Embryo Manipulations

Bilateral ablations of the dorsal 1/3 of the neural tube were performed on HH9 embryos in ovo. Using a glass needle and forceps, a cut was created down the midline from r3 to r5 and the dorsal aspect neural tube was removed. Control embryos were opened, staged and re-sealed. After 24-hour incubation, embryos were treated with BrdU reagent as above for 30 minutes then harvested and processed for immunohistochemistry. To halt proliferation in the mesoderm, Stage HH10 embryos in ovo were injected with a freshly prepared cocktail of 100ug/mL Aphidicolin (A0781, Millipore Sigma), 5mM hydroxyurea (H8627 Millipore Sigma), and 10% DiD. Injections were made at the axial level of r3 to r5 as lateral as could be reached but still in the mesoderm. DiD was used to visualize the area injected and give a rough estimate of where the chemicals were distributed. Control embryos were injected with 10% DMSO and DiD. After injection, embryos were resealed and incubated for 8 hours then fixed and processed for immunohistochemistry. Thirteen injected and eight control embryos were used for analysis.

Microscopy

Live embryos for time lapse imaging were mounted on EC culture dorsal-side down beginning at HH9 or 10 modifying the protocol of (Chapman et al., 2001; McKinney et al., 2016) such that the EC culture was plated with only 500uL of liquid to reduce light scattering. Confocal z-stacks using 488nm laser to image Dendra2 of the transgenic quail and 633 for DiD were collected every 7 minutes for up to 12 hours with a 10x 0.45 objective. Embryos used for photoconversion were mounted similarly on EC culture. Regions approximately 100x100 um for Dendra2 photoconversion were chosen on both sides of the embryo if possible. 5% 405nm laser was scanned in this region and fluorescence intensity of Green Dendra and Red Dendra were monitored in a second channel until the Red intensity no longer increased. A larger, tiled z-stack image of the whole head was then acquired. Embryos were transferred to an incubator for 6 to 8 hours then removed from the culture dish by the paper ring, mounted on a glass slide and immediately re-imaged in a tiled z-stack. Fixed embryos were imaged in 80% FRUIT clearing buffer in tiled, z-stack images with a Plan Apochromat 10x 0.45 NA

objective on an LSM-800 microscope. Microscopy was optimized for imaging AlexaFluor 488, AlexaFluor 546 and methyl green.

Image Analysis

Both in vitro and in vivo time-lapse imaging series were concatenated and aligned (Preibisch et al., 2010) in Fiji (Schindelin et al., 2012). In vivo time-lapses were aligned so that the most dorsal cells at the midline at the center of rhombomere 4 were centered throughout the time-lapses. In this way, multiple movies can be overlaid keeping the spatial information comparable between embryos. Post alignment, images were imported into Imaris (Bitplane AG) for tracking cells with fluorescent labels. In vitro mesoderm and neural crest were tracked by hand due to the single color labeling of the nuclei. If a cell moved into a very dense area or a track could become confused with another cell, the track was stopped. Embryonic cells were tracked semi-automatically with Imaris. Track position and statistics were exported to MATLAB (Mathworks Inc) scripts for further analysis. Distance between random cells (Fig. 2D,F) was calculated only for the time both cells existed. If a division occurred, then one random daughter was picked. Images of BrdU, methyl green and HNK1 labeled embryos were first stitched in Fiji (Preibisch et al., 2009), then imported to Imaris for segmentation. Images were smoothed, attenuation corrected and then the domain around the r4 neural crest stream was isolated by hand. For younger embryos with little or no neural crest present, an area was selected dorsal to the neural tube at the r4 axial level across to the lateral end of the tissue directly across from r4. The width was chosen based on shape of the neural tube. For older embryos, the region of interest was selected from around the neural crest stream down to the most lateral end of the tissue. Similar procedures were followed for the stream of neural crest targeting ba1. The area lateral to r3 was isolated by creating a 100 um circle from the ectoderm between the ba1 and ba2 streams (including the ectoderm). Segmentation was performed on the methyl green signal. Separation of the ectoderm was achieved using a distance transformation to the original domain region and some hand-editing. While the HNK-1 signal is a membrane label, the channel is bright enough to create an intensity cutoff for neural crest identification at the nucleus. The bright BrdU signal allowed us to create an intensity cutoff for

proliferation at the inflection point in a frequency histogram of all BrdU intensities. The average intensity, position and minimum distance to a neighbor were exported to MATLAB scripts for calculating the fraction of cells proliferating and average minimum distance to a neighbor in 50 um bins down the length of the domain. For density measurements, a very rough surface was created in Imaris using the nuclei of cells so that the volume extended to the edge of the tissue. The surface was then cut along the migratory stream at 50um segments. The number of cells located in each segment and the surface volume were used to calculate density. MATLAB scripts can be obtained through Stowers Original Data Repository upon publication.

Computer Model Simulations

We assume that there are two types of cells, namely “leaders” and “followers”. There are a fixed number of leaders who undertake a biased random walk with volume exclusion up a cell-induced gradient of chemoattractant. The leaders perform this biased random walk by extending three filopodia in random directions per time step. These filopodia are assumed able to sense the concentration of chemoattractant at their tip and the cell then moves in the direction of the highest concentration sensed, provided it is higher than that at the position of the center of the cell. If this is not the case, then the cell moves in a random direction. On the other hand, followers are either in a chain or move randomly. A chain consists of a group of followers that are close to each other and at least one of the cells is close to a leader. All the followers in a chain move in the same direction as the leader that is at the front of the chain. If a follower is relatively close to more than one leader so that it may join more than one chain, the cell randomly chooses which one to follow. We include a simplified version of phenotype switching between leaders and followers based on the position of a cell within a migratory stream (see Supplementary Methods).

We use experimental data to parameterize the initial and final lengths of the domain in the model and we carry out three studies. Initially, we consider uniform (U) domain growth throughout the domain. Then we split the domain in two parts, which we call proximal and distal subregions (Fig. 6A), that have different growth rates. We consider

1
2
3
4 first making the difference in growth rates a factor of two (Fig. 6A; Distal (D) and
5 Proximal (P)), and then a combination of distal and proximal growth (Fig. 6A; Mixed
6 (M)). We assume exponential growth of the domain in time and pick the growth rates in
7 such a way that each of the growth profiles leads to the same total domain length after
8 24 hours. We run twenty simulations for each case and store statistics after 24 hours on
9 the density of cells along the domain, the furthest distance travelled (which we quantify
10 as the average maximum distance travelled by the leader cells), and the fraction of the
11 simulations with more than 20% follower cells not in chains (a measure of the likelihood
12 of stream breakage).
13
14
15
16
17
18
19
20
21
22

23 RESULTS

24 **Head mesoderm and neural crest cells in culture are both inherently dynamic but** 25 **the cell behaviors are influenced by co-culture with each other**

26
27 The growth of the vertebrate head is substantial during early development, with
28 proliferation and migration of both mesoderm and neural crest cells (Fig. 1A). To better
29 understand the inherent migratory properties of individual cranial paraxial mesoderm
30 cells, we visualized and quantified cell trajectories of Hoechst-labeled mesoderm
31 isolated from the embryo lateral to rhombomere 4 (r4) at HH6-8 (Hamburger and
32 Hamilton, 1951) (Fig. 1B). Cultured mesoderm cells moved rapidly to disperse
33 throughout the culture dish with an average cell speed of approximately 64 $\mu\text{m/hr}$ and
34 directionality (defined as distance from start to finish divided by the total distance
35 traveled) of 0.22 (Fig. 1C,D). Mesoderm cell behaviors in culture resembled migrating
36 neural crest cells with long, extended cellular processes that stretched between
37 neighboring cells and open spaces of the culture dish (compare Movies 1,2).
38 Occasionally, we observed a few neural crest cells in the mesoderm explant (identified
39 by HNK-1), but typically these cells were absent (Fig. S1).
40
41
42
43
44
45
46
47
48
49
50
51
52
53
54
55
56
57

58 In comparison, cranial neural crest cells that exited from explanted neural tubes moved
59 with an average speed of 79 $\mu\text{m/hr}$ and directionality of 0.19. Neural crest cells were
60
61
62
63
64
65

1
2
3
4 statistically faster and cell trajectories were more circuitous than the mesoderm. We
5 also visually observed that cell exploratory behaviors and interaction of neighbors were
6 similar. However, when we cultured mesoderm and neural tube explants together
7 (Movie 3), both cell types increased their speed to 89 and 86 $\mu\text{m/hr}$, respectively. Only
8 the mesoderm cell speed increased significantly (64 to 89 $\mu\text{m/hr}$; $p=5 \times 10^{-13}$) such that
9 there was relatively no difference in speed between neural crest and mesodermal cells
10 (Fig. 1D). On the other hand, neural crest cells were more directed in the presence of
11 the mesoderm (Fig. 1C). Individual neural crest and mesoderm cells mixed freely, and
12 some neural crest cells infiltrated the explanted intact mesoderm (Movies 3, 4). When
13 we maintained the ectoderm with the intact mesoderm, we found that mesoderm
14 frequently adhered to the sheet of ectoderm and traveled with this tissue (Movie 5).
15 Thus, chick head mesoderm is capable of dissociating and migrating as individual cells.
16 These cells explored the culture dish in a similar manner to neural crest cells but moved
17 faster when neural crest cells were present; neural crest cells responded to the
18 mesoderm by becoming more directed.

31 32 33 34 35 **In vivo time-lapse imaging reveals distinct collective motions of head mesoderm** 36 **and neural crest cell behaviors**

37
38
39 Time-lapse imaging and analysis was performed on the developing head of
40 Tg(hUBC:H2BCerulean-2A-Dendra2) quail embryos (Huss and Lansford, 2017) with
41 premigratory neural crest co-labeled with DiD (Fig. 2A). The neural crest, as well as
42 neighboring mesoderm and ectoderm cell movements, were tracked during neural crest
43 migration (Fig. 2A). Time-lapse movies were aligned so that the dorsal-most cells at the
44 midline in the center of r4 were fixed in position. In this way, multiple movies can be
45 compared while keeping the rough spatial location in the embryo. After the onset of
46 neural crest emigration from r4 in the embryo (approximately HH11), we observed a
47 generally lateral movement of mesoderm and ectoderm cells (Fig. 2A,D,E, Movies 6, 7).
48 After neural crest cells invaded the mesoderm, mesoderm cells migrated with
49 significantly higher directionality of 0.33 than in vitro (0.22), but moved more slowly at
50 approximately 43 $\mu\text{m/hr}$ (Fig. 2B,E). In vivo, the neural crest cells moved through the
51
52
53
54
55
56
57
58
59
60
61
62
63
64
65

mesoderm significantly faster than the mesoderm cells (53 $\mu\text{m/hr}$) and with a significantly higher directionality of 0.40 (Fig 2B,E). By the time that the neural crest cell migratory stream is fully defined adjacent to r4 (HH12), neural crest cells moved at an even faster speed (97.7 $\mu\text{m/hr}$, Fig 2C, Movie 8). In contrast, individual ectoderm cells that directly overlie the dorso-lateral neural crest cell migratory pathway move slowly and are passed by the invading neural crest cells (Movie 8). We sought to find a pattern in the speed or directionality of the cells with respect to location in the embryo and found the speed of the cells near r3 were the slowest tracked, there was not a clear spatial pattern to speed or directionality (Fig. S2).

To quantify the rearrangement of cells during migration, we examined the distance between random pairs of cells at the beginning of the time-lapse to the same cells at the end of the time-lapse session (Fig. 2D). Mesoderm cells were observed to move as a uniform collection of cells; trailing cells did not overtake or leapfrog the leaders and maintained neighbor relationships (Fig. 2D). Mesoderm cells that were far apart, remained far apart as seen with cell pairs distributed along a straight line with slope approximately equal to 1 (Fig. 2D). Similar conclusions can be made of the neural crest which have been shown before to move as a uniform collection of cells without wholesale rearrangement (Fig 2F, (Kulesa et al., 2008)).

Analysis of individual neural crest and mesoderm cell interactions revealed that mesoderm behaviors varied in at least three distinct ways (Fig. 2G, Movie 6). For example, a typical mesoderm cell positioned distal to the neural crest cell invasive front is eventually passed by rapidly moving neural crest cells (Fig. 2G, squares). For two hours, this particular mesoderm cell maintained a straight trajectory parallel to the passing neural crest cells, then changed direction to move posterior near the entrance to the branchial arch. Second, as migrating neural crest cells collided with mesoderm cells, the mesoderm cells were observed to match the neural crest stream direction and move along with the stream as though the cells were pushed (Fig. 2G, circle). Third,

1
2
3
4 some mesoderm cells located very distal to the emerging neural crest cell migratory
5 stream moved slowly enough that neural crest cells leap frogged to move further distally
6 (Fig. 2G, triangle).
7
8
9

10 11 12 13 **Head mesoderm and ectoderm cell proliferation is heterogeneous in space and** 14 **time along the dorsolateral neural crest cell migratory pathway** 15 16

17
18 Considering the large expansion of the head tissue during the stages of neural crest
19 migration (HH9-HH15, 24hours, Fig. 1A), we sought to understand the pattern of cell
20 proliferation and tissue density changes, as well as cell-cell interactions with the neural
21 crest. Previous studies have shown that the growth of the branchial arch is non-uniform
22 over time (McLennan et al., 2012) but to determine the pattern of growth in space, we
23 performed regional photoconversion of mesoderm and ectoderm in vivo. Transgenic
24 quail (HH10) were mounted dorsal side down on EC culture for (Chapman et al., 2001)
25 405nm laser photoconversion of the Dendra2 photoconvertible protein (Fig. 3A,B). A
26 region of interest was drawn roughly 100umx100umx50um and scanned with the
27 405nm laser until the DendraRed signal no longer increased. Embryos were re-
28 incubated for an additional 6-8 hours, imaged, and the dimensions of the
29 photoconverted subregions were re-measured (Fig. 3C). We find that the
30 photoconverted subregions in both mesoderm and ectoderm expanded in the
31 mediolateral direction (along the dorsolateral neural crest migratory pathway and near
32 the neural tube) but remained constant in the dorsal-ventral direction (Fig. 3D). In the
33 anterior-posterior direction (along the vertebrate axis), the photoconverted subregions
34 reduced in size for the mesoderm but remained constant for the ectoderm (Fig. 3D).
35 Together, these data suggest that tissue growth within the paraxial mesoderm and
36 overlying surface ectoderm expands the domain in the proximal-to-distal axis in the
37 direction of neural crest migration more than in orthogonal directions.
38
39
40
41
42
43
44
45
46
47
48
49
50
51
52
53
54
55
56
57

58 To examine the pattern of tissue growth in cellular detail, we studied the distribution of
59 BrdU-labeled mesoderm, ectoderm and neural crest cells between stages HH9 and
60
61
62
63
64
65

1
2
3
4 HH15 to understand if proliferation is a contributor. Pulsed BrdU labeling was executed
5
6 in ovo and we measured the number of BrdU positive cells from confocal z-stacks in
7
8 optically-cleared chick embryos (Fig. 4A). The total number of embryos analyzed for
9
10 each stage is 3 for HH9, 3 for HH11, 5 for HH13 and 5 for HH15. We segmented nuclei
11
12 based on methyl green staining, then categorized the tissue as either ectoderm (by
13
14 distance from the surface), migrating neural crest cells (using HNK-1), or mesoderm
15
16 (Fig. 4B). A cell was categorized as BrdU positive and in S-phase if the intensity was
17
18 above a threshold. We find that overall, between HH9 and HH15, there is substantial
19
20 inhomogeneity in BrdU labeling in space and time (Fig 4A, F- H). For instance, at HH9,
21
22 there are fewer cells in S-phase near the midline and the staining increases in
23
24 frequency more laterally (Fig. 4A,G). By HH13-15 there are many subregions of high or
25
26 low BrdU labeling. We next specifically examined the percentage of BrdU-positive
27
28 mesodermal cells along the dorsolateral neural crest cell migratory pathway from r4 to
29
30 ba2 in 50 um bins starting at the midline to the end of the tissue (Fig. 4C-H). We found
31
32 that the fraction of BrdU-positive mesodermal cells was highest in the subregion distal
33
34 to the invasive neural crest cells within a range of approximately 100 um in length,
35
36 beginning prior to neural crest cell exit from the mid-r3 to mid-r4 neural tube and
37
38 through to HH15 (Fig. 4G, dashed line).
39
40

41 At HH15, the BrdU pattern changes to be higher in the paraxial mesoderm near the
42
43 dorsal neural tube midline and uniform throughout the remainder of tissue towards ba2.
44
45 Similar measurements were performed on the tissue moving towards ba1 for
46
47 comparison (Fig. 4C,F, Fig. S3). Along the neural crest cell migratory pathway towards
48
49 ba1, the fraction of BrdU-positive cells was higher in the distal subregion at HH9, but
50
51 this pattern becomes homogeneously distributed along the dorsolateral pathway from
52
53 HH11-13 (Fig. S3). We measured a small increase in BrdU labeling in mesodermal cells
54
55 in the paraxial mesoderm adjacent to rhombomere 1 (r1) at HH15 (Fig S3). Also, we
56
57 also measured the fraction of BrdU-positive mesodermal cells in the region distal to r3
58
59 (Fig. 4D,F). Branchial arches 1 and 2 protrude outward from the embryo while this
60
61 region does not extend as much. A smaller fraction of these cells are BrdU labeled
62
63
64
65

1
2
3
4 between stages HH9-HH13 but the fraction increases at HH15 to be more similar to the
5 proliferation in ba1. Similarly, we measured the BrdU labeling in the surface ectoderm
6 overlying the path from near r4 to ba2 and found a higher percentage of cells were
7 labeled with BrdU between stages HH9 and HH13 (Fig. 4F,H). In contrast to the
8 mesoderm, the BrdU labeling was more or less constant throughout the region, with the
9 exception of HH11, where there is a higher fraction of cells labeled towards the lateral
10 edge of the tissue (Fig. 4H).
11
12
13
14
15
16
17
18
19
20

21 **Cell density remains constant within proliferating mesoderm implying tissue** 22 **growth expansion** 23

24
25 To address whether cell proliferation of the head mesoderm translates into an increase
26 in local cell density and/or an increase in tissue size, we measured the nearest neighbor
27 distance between every detected cell nuclei within the mesoderm between HH9 and 15
28 (Fig. 5A,B). We find that the subregions of high BrdU label do not coincide with higher
29 cell density (Fig. 5A, orange cells). The average distance to each cell's nearest
30 neighbor was calculated for each stage (Fig. 5C) and in 50um bins along the
31 dorsolateral pathway (Fig. 5D,E). We attempted to also measure actual density within
32 the tissue (Fig. S4) but due to the inaccuracies in measuring volume, we feel the
33 nearest neighbor distance is more accurate. Using the nearest neighbor distance as a
34 proxy for density, we find that the cell density is relatively constant through the
35 subregion (Fig. 5D), with the exception of HH11. At HH9, mesodermal cells are tightly
36 packed with an average of only 10 um, or a typical cell nucleus length, between
37 neighbors (Fig. 5C,D). As the tissue grows, mesodermal cells become less dense at
38 HH11 and HH13 (24 um and 21 um between neighbors on average, respectively) but
39 pack in more tightly again by HH15 (13 um). The ectoderm is, in general, more packed
40 with cells than the mesoderm and does not vary through stages or with spatial
41 location(Fig. 5E). A schematic describing the neural crest stream development,
42 proliferation and density can be found in Fig. 5F. These data support the concept that
43 mesodermal cell proliferation gives rise to tissue growth since the areas of high BrdU
44 labeling coincide with more loosely packed mesoderm.
45
46
47
48
49
50
51
52
53
54
55
56
57
58
59
60
61
62
63
64
65

Computer model simulations reveal a modest change in neural crest cell speed is required to respond to non-uniform domain growth

The non-uniform expansion and density variations of the mesoderm as determined above plus the faster and more directed nature of the in vivo neural crest cells creates a unique problem set for the collective migration of the neural crest. To explore the effects of non-uniform domain growth profiles on the neural crest cell migratory pattern, we exploited the strengths of our computer model (Fig. 6). We considered three distinct non-uniform domain growth profiles in which the domain growth was twice as fast within either the proximal or distal subregions of the domain (Fig. 6A). Specifically, we considered domain growth on the distal half of the domain (Fig. 6A; Distal (D)), the proximal half of the domain (Fig. 6A; Proximal (P)), and a combination of distal and proximal growth to mimic the empirically measured data presented in Fig. 4 (Fig. 6A; Mixed (M)). Each simulation was run for 24 hrs embryonic time and measurements were collected. In all simulations, the distribution of neural crest cells was measured at 24 hrs (Fig. 6B).

In the scenario of increased distal domain growth, the model predicts that the furthest distance traveled by cells is reduced in comparison with the uniform growth (Fig. 6A; compare U vs. D). In contrast, when the proximal subregion of the domain grows twice as fast compared to the distal subregion, the model predicts that cells travel further than with the uniform domain growth profile (Fig. 6A; compare U vs P). By combining the distal and proximal growth profiles to align with the empirical measurements where early there is more distal growth and at 18 hours, the growth switches to proximal (Fig. 4), we find the model predicts that there must be an increase in input neural crest cell speed in order for cells to reach the domain in 24 hrs (Fig. 6A; see mixed (M) with cell speed $s=48$ $\mu\text{m/hr}$). The neural crest have two speed components: the input speed (Fig. 6) as well as an advection speed as they are carried by the domain growth. When input neural crest cell speed is increased, the stream length monotonically increases (Fig.

6B). This may be clarified by visualizing the changes in neural crest cell overall speed from the neural tube exit as a function of increasing cell speed from 42 $\mu\text{m/hr}$ to 51 $\mu\text{m/hr}$ (Fig. 6B). Note that if the neural crest cell speed is increased too high to 51 $\mu\text{m/hr}$, the neural crest cells have to slow their speed during the last portion of migration so as not to over shoot the target (Fig. 6B). Together, the model simulations predict that neural crest cells must undergo a modest increase in cell speed from 42 to 48 $\mu\text{m/hr}$ (approximately 14%) in order to reach near to the end of the migratory domain.

The pattern of cell proliferation and tissue growth of the head mesoderm is altered after ablation of premigratory neural crest cells

With our observed changes in mesoderm cell speed and directionality in culture in the presence of neural crest cells and heterogeneity of tissue growth in space and time, we sought to better understand the influence of migrating neural crest cells on this pattern. To address this, we ablated the dorsal one-third of the neural tube in a bilateral manner from mid-r3 to mid-r5 in HH9 embryos to significantly reduce the number of premigratory neural crest cells (Fig. 7A). After 24 hrs of egg re-incubation to HH15, BrdU labeling was applied in ovo before embryos were harvested, fixed and processed for immunolabeling of the migrating neural crest cells with HNK-1. In silico, we ran simulations of the ablation of premigratory neural crest by reducing the number of migrating cells (to accurately capture some cells that escape ablation in the experiment) and delay before entering the domain, using the mixed (M) growth profile above (Fig. 7A, right). We measured the distal length from the neural tube midline to the brachial arches along the presumptive dorsolateral neural crest cell migratory pathway, and found this distance was significantly reduced in ablated embryos in comparison to controls (Fig. 7B). Simulations showed that the ratio of the migratory domain length to neural crest cell stream front was also reduced (Fig. 7B; red/green bars). Examination of the pattern of BrdU-labeled mesodermal cells revealed that cell proliferation was higher along the length of the domain at every position and, at the distal-most locations increased by 24% (Fig. 7A,C).

1
2
3
4
5
6
7 It has been shown that the surface ectoderm expresses VEGF which is a proliferative
8 inducing agent as well as a chemoattractant for the neural crest (McLennan et al.,
9 2010). Without the neural crest population binding to the VEGF expressed by the
10 ectoderm, we examined the effects of increased VEGF on the mesoderm population by
11 exposing mesoderm in culture to 100ug/mL VEGF. We found a significant increase in
12 the percentage of dividing mesoderm cells (Fig. 7D,E). Thus, in the absence of
13 migrating neural crest as in ablated embryos, increased proliferation of the mesoderm
14 could be stimulated by increased exposure to VEGF.
15
16
17
18
19
20
21

22 **Inhibition of mesoderm cell proliferation reduced domain size and length of the** 23 **neural crest cell migratory stream** 24 25 26

27 The computer model simulations presented above predicted significant changes in the
28 neural crest cell migratory distance depending on the domain growth profile (Fig. 6A).
29 To attempt a change in growth rate in vivo, we microinjected a cocktail of Aphidicolin
30 (1mg/mL), Hydroxyurea (5mM) and DiD into the most lateral mesoderm that could be
31 reached in HH10 embryos (Fig. 7F). Aphidicolin and hydroxyurea are both well-known
32 to inhibit the cell cycle in S-phase and halt proliferation (Levenson and Hamlin, 1993;
33 Mutomba and Wang, 1996). We microinjected control embryos with 10% DMSO and
34 DiD. All microinjected embryos were re-incubated for 8 hrs then labeled with HNK1 to
35 fluorescently label migrating neural crest and methyl green to mark all cells (Fig. 7F).
36 While we anticipate the chemicals to spread further than the DiD marked area, we also
37 anticipate that in only 8 hours of re-incubation, the subregions with higher fractions of S-
38 phase cells marked with BrdU (from Fig. 4G,H) will be most highly affected. That is, the
39 most lateral parts of the mesodermal domain will be halted in S-phase. In silico, we
40 modeled the inhibition by reducing domain growth throughout the two-dimensional
41 space (Fig. 7F). We find that both the mesoderm within the dorsolateral domain and
42 neural crest cell migratory stream were shorter in experimentally treated embryos (Fig.
43 7G). The ratio of the length of the neural crest cell migratory stream to the total length of
44 the branchial arch tissue was significantly reduced (Fig. 7G). In contrast, in simulation of
45 inhibited domain growth, the ratio of the neural crest cell migratory stream to the domain
46
47
48
49
50
51
52
53
54
55
56
57
58
59
60
61
62
63
64
65

length increased in the presence of an inhibitor (Fig. 7G; red/green bars). This could be explained in that our model does not include a feedback mechanism between the neural crest and mesoderm so the neural crest are able to continue their migratory program unphased by the size or growth rate of the domain and travel further into the stream. Thus, by chemically inhibiting cell proliferation in the mesoderm (and probably ectoderm), we were able to reduce tissue growth but, more importantly, alter the resulting neural crest stream length.

In vivo time-lapse imaging reveals distinct collective motions of head mesoderm and ectoderm cell behaviors prior to neural crest emergence

The in vivo time-lapse measurements of neural crest and mesoderm interactions, speed and directionality beg the analysis of the mesoderm before the neural crest emerge near r4. When embryos were imaged prior to neural crest emergence, we observed a few interesting phenomena (Fig 8). First, as neural crest cells are emerging from the neural tube and beginning to migrate, the ectoderm can be seen to bend and change shape as the embryo grows (Fig. 8A and Movie 9). The large morphological changes to the embryo alter the presumptive path of the neural crest, from at first being relatively straight, to a curved path following the ectoderm deflection. Second, mesoderm and ectoderm cells adjacent to the dorsal hindbrain moved in a counter-clockwise whirling pattern prior to the emergence of neural crest cells (Fig.8B-D, Movie 7). The whirling pattern of cells was observed in 7 of 12 embryos when the time-lapse was begun before 10 somite stage. The whirling pattern had a diameter of approximately 125 μm and was centered adjacent to r3. Mesoderm and ectoderm cells rotated together at 0.2 degrees per minute, suggesting that one revolution would take approximately 30 hrs to complete and cannot be fully visualized here. The whirling cells were at least 50 μm deep into the tissue but the maximum depth could not be determined due to the lack of light penetration into the tissue. Interestingly, the whirling behaviors of the mesoderm and ectoderm stopped coincident with the emergence of the r4 neural crest cells (Movie 7). Further, the pattern of mesoderm cell behaviors on the left-hand side of the embryo rotated in a clockwise manner (data not shown). The whirling effect was not observed in

other locations or at later time points. Cell tracking and analysis showed that mesoderm cells 'before' neural crest emergence moved at 46 $\mu\text{m/hr}$ on average with directionality of 0.21 which is slower and less directed than 'after' neural crest cells emerged (Fig. 8E-F).

DISCUSSION

Previous static studies have suggested that head mesoderm (through which neural crest cells travel) grows in a uniform manner in space (McLennan et al., 2012) and neural crest cells are passively carried along (Noden and Trainor, 2005; Evans and Noden, 2006) rather than actively migrating. Our discovery of the inherent motility of individual mesoderm cells in culture, and dramatic changes in cell behaviors in the presence of cranial neural crest cells, suggested a more complex and dynamic choreography of vertebrate head morphogenesis. In vivo imaging and experiments demonstrated the rich spatio-temporal pattern of ectoderm and mesoderm cell dynamics, and cell-cell interactions with migrating neural crest cells. Mathematical model simulations of variable domain growth profiles confirmed the robustness of cranial neural crest migration in the complex environment of the growing domain. Overall, we present a descriptive analysis showing neural crest and mesoderm can behave as independent migratory populations but are influenced by the presence and behavior of each other.

Head mesodermal cells in culture displayed inherent dynamic migratory behaviors in vitro, suggesting these cells are capable of active cell movements in vivo and could exchange of neighbor relationships. Mesodermal cells isolated from the chick head paraxial mesoderm adjacent to the rostral hindbrain dispersed as individuals throughout the culture dish in a similar manner to neural crest cells that exit cultured neural tube explants (Fig. 1). Mesodermal cells in culture moved 81% slower but 155% more directed than neural crest cells in vitro (Fig. 1). This was surprising since paraxial and lateral mesoderm have previously been assumed as passive tissue (Noden and Trainor,

2005; Evans and Noden, 2006). Interestingly, when placed in co-culture with neural crest cells, both mesoderm and neural crest cells migrated faster and freely intermingled (Fig. 1). Thus, the inherent motility of head mesoderm cells and dynamic interplay with the neural crest and ectoderm in culture, mean that cell behaviors must be closely coordinated in vivo to create the stereotypical pattern of the head and branchial arches.

In the embryo, mesodermal cells displayed directed mediolateral motion and interacted with invading neural crest cells, suggesting a close coordination between the neural crest and mesodermal cells to expand tissue growth and morphogenesis of the branchial arches. Unlike in vitro, the mesoderm cells moved as a collective, keeping spatial order. Both cell types moved more slowly in vivo, most likely due to the presence of extracellular matrix components, other cell types and three-dimensional spatial restrictions. As in vitro, mesoderm cells that interacted with neural crest cells displayed more directed cell trajectories (Fig. 1, Fig. 2G, circles) however, instead of mixing, some mesoderm cells were displaced either lateral or off the migratory pathway after interacting with a neural crest cell (Fig. 2G, triangle). The fact that neural crest and mesoderm cells interacted was not surprising given previous data from quail-chick chimeras or viral labeling studies that reported populations of these two cell types developed in close registration (summarized in (Le Douarin and Kalcheim, 1999); reviewed in (Noden and Trainor, 2005)). However, it was stunning to observe the rich individual mesoderm and neural crest cell-cell interactions and rapid movements of neural crest cells to overtake individual mesoderm cells en route to the branchial arches (see Movie 6). We did not observe neural crest cells to be solely carried along passively by the underlying moving mesoderm tissue (Evans and Noden, 2006), but this may occur later during branchial arch patterning. Intriguingly, neural crest cells that were observed to displace loosely-connected mesoderm cells would require cell contact with enough force to change the direction of the contacted cell. Further time-lapse studies that focus on local mesoderm and neural crest cell-cell interactions combined with an examination of the expression of cell receptor-ligand pairs should help to better

1
2
3
4 understand the dynamic relationship between these two cell types and the transition of
5 the mesoderm cells to lateral movement.
6
7
8
9

10
11 Mesoderm tissue growth is non-uniform in space and differs from the ectoderm,
12 suggesting more complex cell dynamics than previously thought. Photoconversion of
13 small volumes of paraxial mesoderm tissue (Fig. 3) showed the tissue is expanding in
14 the lateral direction more than in any other direction. BrdU-positive cell numbers
15 increased laterally through the mesoderm domain between HH9 and HH13 that hinting
16 that there was higher cell proliferation towards the lateral end of the domain; the density
17 of the cells remained constant (Fig. 4; with the exception of HH11). In addition, our
18 time-lapse movies show a flow of mesoderm cells towards the lateral end of the domain
19 without major cell rearrangements, leapfrogging or circulation (Fig. 2A) implying tissue
20 expansion is driven by proliferation and lateral movement of the mesoderm. The
21 ectoderm overlying the mesoderm domain had an even higher fraction of cells positive
22 for BrdU, but in general is a more densely packed tissue such that every division may
23 not result in expansion. We conclude that the mesoderm is therefore the main driver of
24 growth in the lateral direction pushing the branchial arch formation. Comparing the area
25 adjacent to r3, where there is less expansion, a smaller fraction of mesoderm cells are
26 positive for BrdU and the tissue is denser until stage 15 when the arches are poised to
27 fuse together and perhaps another pattern of growth could be taking shape.
28
29
30
31
32
33
34
35
36
37
38
39
40
41
42
43
44
45

46 Despite the non-uniformity in tissue growth in space and time, migrating neural crest
47 cells remained as a continuous stream of cells. Interestingly, our data indicated that
48 during neural crest migration to the branchial arches (HH11-15) the mesoderm is
49 proliferating ahead of the neural crest migratory front (Figs. 4G, 5F; highest fraction of
50 BrdU positive cells beyond the neural crest stream). Neural crest cells must then
51 actively migrate to stay in pace with the branchial arches (Fig. 5F). In analogy, the
52 neural crest cells are on a moving walkway in which the different sections of the
53 walkway move faster/slower over time. How the neural crest cells modulate advection
54
55
56
57
58
59
60
61
62
63
64
65

and active migration while traveling through the mesoderm will be exciting to examine mechanistically in the future.

Computational modeling allowed us to rapidly compare the effect of non-uniform domain growth on the neural crest stream pattern and test the hypothesis that cells must change speed to compensate. When we tested either enhanced growth of the distal-half (D) or proximal-half (P) of the domain, we learned that the stream length was longer with proximal growth since the neural crest cells were able to be advected by the domain for longer periods of time. However, distal growth of the domain more accurately captured our empirical data (for the first 18 hrs of neural crest migration) and the resulting shortened neural crest stream suggested cells must increase speed to compensate (Fig. 6A). By combining the empirically measured proximal domain growth into the simulation for the last portion of the process (from 18-24 hrs), this promoted the follower cells to maintain the collective stream migration (Fig. 6A). When we tested the change in cell speed to compensate for domain growth, we found that an increase from 42 to 48 $\mu\text{m/hr}$ (approximately 14%) was adequate for the stream to reach nearly the end of the domain in 24 hrs (Fig. 6B). Together, this suggests that neural crest cell migration is a combination of advection and active migration with only a modest increase in cell speed required for the neural crest to compensate for non-uniform tissue growth over a 24hrs period of migration.

The pattern of BrdU staining and tissue growth of the head mesoderm was altered after ablation of premigratory neural crest cells, suggesting VEGF (or other growth factor signals) promotes both neural crest migration and mesoderm proliferation simultaneously. After ablation of premigratory r4 neural crest cells, ba2 formed but was smaller than in control embryos (Fig. 7A,C) agreeing with previously published observations that branchial arch tissue can form independent of the neural crest cells (Veitch et al., 1999). A large fraction of the tissue in the branchial arches is composed of neural crest cells (Fig. 1A) so to make up the volume lost after the ablation, we

1
2
3
4 reasoned that the mesoderm must increase in its proliferation (Fig. 7C). When we
5 simulated the ablation of premigratory neural crest cells, we learned that the domain
6 length was unaffected and cells that escaped ablation did not reach the end of the
7 normal growing domain since the model does not have a feedback mechanism between
8 the mesoderm and neural crest (Fig. 7A,B). To consider this, we suggest that VEGF
9 may have a dual role to act as a chemoattract for the neural crest (McLennan and
10 Kulesa, 2010; McLennan et al., 2010) and as a proliferative agent. We found that
11 cultured mesodermal cells overproliferated in response to VEGF added to the media
12 (Fig. 7D,E). These data support previous observations that branchial arch tissue can
13 form independent of the neural crest cells and suggest the increase in proliferation of
14 mesodermal cells may result from an overabundance of VEGF. However, the
15 downstream morphogenesis of muscle and bone would still be affected (Noden, 1988;
16 Veitch et al., 1999). It is possible that there are other signals or growth factors
17 originating in the dorsal neural tube that could influence either the proliferation or cell
18 motion of the mesoderm that were ablated with the neural crest, however presence of
19 VEGF has already been established and seems a likely candidate (McLennan et al.,
20 2010). If the VEGF, or other factor, induces the growth of the mesoderm at r4, then it
21 might stand to reason that the same factor could be acting adjacent to r3 where there
22 are no neural crest cells but there are less proliferating cells in this region (Fig. 4F).
23 However, a BMP inhibitor, DAN (NBL1), was found in the area adjacent to r3 and
24 inhibits proliferation in neural crest (McLennan et al., 2017). It is possible that there are
25 other mechanisms at work in the area adjacent to r3 to repress the growth of the cleft
26 between the arches.

27
28
29
30
31
32
33
34
35
36
37
38
39
40
41
42
43
44
45
46
47
48
49
50 We also asked the converse question, if the branchial arches were to diminish in size,
51 what effect would this have on the migratory neural crest stream? Chemical inhibition of
52 cell proliferation in the mesoderm led to reduced length of ba2, but the neural crest cell
53 migratory stream length was also significantly reduced (Fig. 7F,G). We expected the
54 neural crest cells to travel further into the branchial arch with a shorter domain following
55 their own program for invasion and proliferation in the branchial arches. However, since
56
57
58
59
60
61
62
63
64
65

1
2
3
4 the neural crest cells traveled a shorter distance through the migratory domain (Fig.
5 7F,G), this implied a signaling interplay between the independent motion of the neural
6 crest and growth activity of the mesoderm or ectoderm. Future model simulations that
7 test hypothetical feedback mechanisms between the neural crest and mesoderm to
8 either stimulate or inhibit growth and migration will help to shed light on this question.
9
10
11
12
13
14
15
16

17 Another interesting result of our time lapse studies was the behavior of the ectoderm
18 and mesoderm cells prior to neural crest migration. The cells displayed large scale
19 collective whirling motions lateral to r3 (prior to neural crest cell emergence). Whirling
20 patterns of cells have been observed in many contexts, from confluent fibroblast
21 cultures (Elsdale and Wasoff, 1976) to vertebrate gastrulation in the tailbud of zebrafish
22 and chick embryos, especially within the mesodermal progenitor zone (MPZ) (Zamir et
23 al., 2006; Lawton et al., 2013; Mongera et al., 2018). Curiously, the observance of a
24 large scale, circular structure has previously been reported in chick head mesoderm
25 and visualized using stereo scanning electron microscopy (Meier, 1981; Jacobson,
26 1988). They reported paired mesodermal cell disks, which they termed 'somitomes,'
27 with a diameter ranging from 135 to 240 μm , appearing in an anterior-to-posterior order
28 starting at about HH4 through HH9. Cells were arranged around one or two central cells
29 with a tuft of processes pointing toward the ectoderm (Meier, 1981; Jacobson, 1988).
30 When we measured ectoderm and mesoderm cell movements within presumed
31 somitomes, we found that cells traveled in a counter-clockwise direction on the right-
32 hand-side of the embryo (and clockwise on left-hand-side) at a speed of 0.2 degrees
33 per minute (Fig. 8B-D). Further analysis of mesodermal cell-cell interactions and
34 changes in tissue boundary geometries or molecular signals in the microenvironment in
35 the vertebrate head should help us better understand the functional relationship
36 between whirling motions, tissue growth, and the emergence of the migrating neural
37 crest cells.
38
39
40
41
42
43
44
45
46
47
48
49
50
51
52
53
54
55
56
57
58
59
60
61
62
63
64
65

1
2
3
4 In conclusion, our results support a model wherein neural crest cells balance active
5 motility and growth-driven advection to preserve movement as a collective cell
6 population. Paraxial mesodermal cells are inherently motile and display collective cell
7 movements that transition from large-scale whirling (prior to neural crest cell
8 emergence) to directed trajectories towards the branchial arches. By simultaneously
9 observing ectoderm, mesoderm and neural crest cell behaviors, we have unraveled the
10 complex cell dynamics that lead to head and branchial arch morphogenesis. Empirical
11 measurements revealed spatiotemporal changes in tissue growth expansion that begin
12 within the paraxial mesoderm and transition to the distal subregion of the forming
13 branchial arches over time. By simulating neural crest cell migration in response to the
14 experimentally measured tissue growth profile, we arrived at a better understanding of
15 changes in neural crest cell speed to compensate. Our manipulation of the neural crest
16 cell migratory domain by ablation of the premigratory neural crest or inhibition of
17 mesodermal cell proliferation strengthen the idea that interactions between the two cell
18 populations stimulate tissue growth. Lastly, our detailed analysis of avian head
19 morphogenesis and neural crest cell migration now provide a framework to integrate
20 single cell genomic data and comparisons between different vertebrate research
21 organisms.
22
23
24
25
26
27
28
29
30
31
32
33
34
35
36
37
38
39
40
41
42
43
44
45
46
47
48
49
50
51
52
53
54
55
56
57
58
59
60
61
62
63
64
65

ACKNOWLEDGEMENTS

PMK would like to acknowledge the kind and generous funding from the Stowers Institute for Medical Research. We would also like to thank David Huss, Rusty Lansford, and the Translational Imaging Center at the University of Southern California for use of the transgenic quail. In addition, we thank Dave Lei and Ashley Young for contributions to imaging and image analysis as part of the Stowers Summer Scholars Program.

COMPETING INTERESTS

No competing interests declared

FUNDING

This work was supported by the kind funding of The Stowers Institute for Medical Research. R.E.B. is a Royal Society Wolfson Research Merit Award holder. H.G.O. is supported by National Institutes of Health award RO1GM029123.

DATA AVAILABILITY

Original data underlying this manuscript can be accessed from the Stowers Original Data Repository at <https://www.stowers.org/research/publications/odr>

REFERENCES

- Chapman, S. C., Collignon, J., Schoenwolf, G. C. and Lumsden, A. (2001) 'Improved method for chick whole-embryo culture using a filter paper carrier', *Dev Dyn* 220(3): 284-9. doi:T10.1002/1097-0177(20010301)220:3
- Elsdale, T. and Wasoff, F. (1976) 'Fibroblast cultures and dermatoglyphics: The topology of two planar patterns', *Wilehm Roux Arch Dev Biol* 180(2): 121-147. doi:T10.1007/BF00848102
- Evans, D. J. and Noden, D. M. (2006) 'Spatial relations between avian craniofacial neural crest and paraxial mesoderm cells', *Dev Dyn* 235(5): 1310-25. doi:T10.1002/dvdy.20663
- Hacker, A. and Guthrie, S. (1998) 'A distinct developmental programme for the cranial paraxial mesoderm in the chick embryo', *Development* 125(17): 3461-72.
- Hamburger, V. and Hamilton, H. (1951) 'A series of normal stages in the development of the chick embryo', *J Morph* 88(1): 49-92. doi:T10.1002/jmor.1050880104
- Hou, B., Zhang, D., Zhao, S., Wei, M., Yang, Z., Wang, S., Wang, J., Zhang, X., Liu, B., Fan, L. et al. (2015) 'Scalable and Dil-compatible optical clearance of the mammalian brain', *Front Neuroanat* 9: 19. doi:T10.3389/fnana.2015.00019
- Huss, D. and Lansford, R. (2017) 'Fluorescent Quail: A Transgenic Model System for the Dynamic Study of Avian Development', *Methods Mol Biol* 1650: 125-147. doi:T10.1007/978-1-4939-7216-6_8
- Jacobson, A. G. (1988) 'Somitomers: mesodermal segments of vertebrate embryos', *Development* 104 Suppl: 209-20.
- Kontges, G. and Lumsden, A. (1996) 'Rhombencephalic neural crest segmentation is preserved throughout craniofacial ontogeny', *Development* 122(10): 3229-42.
- Kulesa, P. M. and McLennan, R. (2015) 'Neural crest migration: trailblazing ahead', *F1000Prime Rep* 7: 02. doi:T10.12703/P7-02
- Kulesa, P. M., Teddy, J. M., Stark, D. A., Smith, S. E. and McLennan, R. (2008) 'Neural crest invasion is a spatially-ordered progression into the head with higher cell proliferation at the migratory front as revealed by the photoactivatable protein, KikGR', *Dev Biol* 316(2): 275-87. doi:TS0012-1606(08)00064-X [pii]10.1016/j.ydbio.2008.01.029
- Lawton, A. K., Nandi, A., Stulberg, M. J., Dray, N., Sneddon, M. W., Pontius, W., Emonet, T. and Holley, S. A. (2013) 'Regulated tissue fluidity steers zebrafish body elongation', *Development* 140(3): 573-82. doi:T10.1242/dev.090381
- Le Douarin, N. and Kalcheim, C. (1999) *The neural crest*, Cambridge, UK ; New York, NY, USA: Cambridge University Press.
- Levenson, V. and Hamlin, J. L. (1993) 'A general protocol for evaluating the specific effects of DNA replication inhibitors', *Nucleic Acids Res* 21(17): 3997-4004.
- McKinney, M. C., McLennan, R. and Kulesa, P. M. (2016) 'Angiopoietin 2 signaling plays a critical role in neural crest cell migration', *BMC Biol* 14(1): 111. doi:T10.1186/s12915-016-0323-9
- McLennan, R., Bailey, C. M., Schumacher, L. J., Teddy, J. M., Morrison, J. A., Kasemeier-Kulesa, J. C., Wolfe, L. A., Gogol, M. M., Baker, R. E., Maini, P. K. et al. (2017) 'DAN (NBL1) promotes collective neural crest migration by restraining uncontrolled invasion', *J Cell Biol* 216(10): 3339-3354. doi:T10.1083/jcb.201612169
- McLennan, R., Dyson, L., Prather, K. W., Morrison, J. A., Baker, R. E., Maini, P. K. and Kulesa, P. M. (2012) 'Multiscale mechanisms of cell migration during development: theory and experiment', *Development* 139(16): 2935-44. doi:T10.1242/dev.081471
- McLennan, R. and Kulesa, P. (2010) 'Neuropilin-1 interacts with the second branchial arch microenvironment to mediate chick neural crest cell dynamics', *Developmental dynamics : an official publication of the American Association of Anatomists* 239(6): 1664-1673. doi:T10.1002/dvdy.22303

- 1
2
3
4 McLennan, R., Teddy, J. M., Kasemeier-Kulesa, J. C., Romine, M. H. and Kulesa, P. M. (2010) 'Vascular
5 endothelial growth factor (VEGF) regulates cranial neural crest migration in vivo', *Dev Biol* 339(1):
6 114-25. doi:T10.1016/j.ydbio.2009.12.022
- 7
8 Meier, S. (1981) 'Development of the chick embryo mesoblast: morphogenesis of the prechordal plate
9 and cranial segments', *Dev Biol* 83(1): 49-61.
- 10 Mongera, A., Rowghanian, P., Gustafson, H. J., Shelton, E., Kealhofer, D. A., Carn, E. K., Serwane, F.,
11 Lucio, A. A., Giammona, J. and Campas, O. (2018) 'A fluid-to-solid jamming transition underlies
12 vertebrate body axis elongation', *Nature* 561(7723): 401-405. doi:T10.1038/s41586-018-0479-2
- 13
14 Mutomba, M. C. and Wang, C. C. (1996) 'Effects of aphidicolin and hydroxyurea on the cell cycle and
15 differentiation of Trypanosoma brucei bloodstream forms', *Mol Biochem Parasitol* 80(1): 89-102.
- 16 Noden, D. (1988) 'Interactions and fates of avian craniofacial mesenchyme', *Development (Cambridge,*
17 *England)* 103 Suppl: 121-140.
- 18 Noden, D. and Trainor, P. (2005) 'Relations and interactions between cranial mesoderm and neural crest
19 populations', *Journal of anatomy* 207(5): 575-601. doi:T10.1111/j.1469-7580.2005.00473.x
- 20
21 Preibisch, S., Saalfeld, S., Schindelin, J. and Tomancak, P. (2010) 'Software for bead-based registration of
22 selective plane illumination microscopy data', *Nat Methods* 7(6): 418-9. doi:Tnmeth0610-418
23 [pii]10.1038/nmeth0610-418
- 24
25 Preibisch, S., Saalfeld, S. and Tomancak, P. (2009) 'Globally optimal stitching of tiled 3D microscopic
26 image acquisitions', *Bioinformatics* 25(11): 1463-5. doi:T10.1093/bioinformatics/btp184
- 27
28 Prieto, D., Aparicio, G., Machado, M. and Zolessi, F. R. (2015) 'Application of the DNA-specific stain
29 methyl green in the fluorescent labeling of embryos', *J Vis Exp*(99): e52769. doi:T10.3791/52769
- 30
31 Schindelin, J., Arganda-Carreras, I., Frise, E., Kaynig, V., Longair, M., Pietzsch, T., Preibisch, S., Rueden, C.,
32 Saalfeld, S., Schmid, B. et al. (2012) 'Fiji: an open-source platform for biological-image analysis', *Nat*
33 *Methods* 9(7): 676-82. doi:T10.1038/nmeth.2019
- 34
35 Szabo, A. and Mayor, R. (2016) 'Modelling collective cell migration of neural crest', *Curr Opin Cell Biol* 42:
36 22-28. doi:T10.1016/j.ceb.2016.03.023
- 37
38 Tosney, K. W. (1982) 'The segregation and early migration of cranial neural crest cells in the avian
39 embryo', *Dev Biol* 89(1): 13-24.
- 40
41 Veitch, E., Begbie, J., Schilling, T. F., Smith, M. M. and Graham, A. (1999) 'Pharyngeal arch patterning in
42 the absence of neural crest', *Curr Biol* 9(24): 1481-4.
- 43
44 Zamir, E. A., Czirok, A., Cui, C., Little, C. D. and Rongish, B. J. (2006) 'Mesodermal cell displacements
45 during avian gastrulation are due to both individual cell-autonomous and convective tissue
46 movements', *Proc Natl Acad Sci U S A* 103(52): 19806-11. doi:T10.1073/pnas.0606100103
- 47
48
49
50
51
52
53
54
55
56
57
58
59
60
61
62
63
64
65

FIGURE LEGENDS

Figure 1: Growing chick embryo and mesodermal cell migration. (A) Similarly scaled chick embryos between stages HH9 and HH15 showing the growth of the head. All nuclei (green) and neural crest (magenta) illustrate the increase in number of cells and size of the embryo over time. Upper images: lateral view, scale bar 150um. Lower images: transverse view at the level of r4, scale bar 50um. (B) Column 1: Mesodermal cells isolated from HH6-8 embryos grown in vitro. Final panel are tracks of individual cells over 10 hours. Column 2: Neural tube from HH11 embryo cultured. Final panel tracks of neural crest cells. Column 3: Neural tube from HH11 embryo co-cultured with mesoderm sample. Final panel are tracks of neural crest cells (magenta) and mesoderm (green). Scale bars 50um. (C) Directionality and (D) Speed of mesoderm only (green, n=5, 94 cells total), neural crest cells only (magenta, n=4, 73 cells), mesoderm cells in the presence of neural crest (green markers with magenta box, n=3, 91 cells) and neural crest in the presence of mesoderm (magenta markers with green box, n=3, 66 cells).

Figure 2: Neural crest cells are faster and more directed than the surrounding mesoderm in vivo. (A) Schematic of a typical embryo mounted with EC culture media. Images of Dendra2 (green) transgenic quail roughly HH13 or 9 hours into a time-lapse session with DiD labeling of premigratory neural crest (magenta). First image of example time-lapse with r4 and edge of neural tube marked. First image overlayed with tracks of mesoderm/ectoderm cells colored by time and neural crest cells in magenta. Scale bars 100um. Directionality (B) and Speed (C) of neural crest, mesoderm and ectodermal cells. n=3 embryos each, 242 mesoderm/ectoderm cells and 74 neural crest. (D) Comparison of the separation distance between any two mesoderm cell pairs at the time of their first co-existence to their last observation, including pairs from different time-lapse movies. Straight line fit to data (dashed black). (F) Separation distance for neural crest only. (E) Transverse view of r4 at HH12. Individual ectoderm cells (cyan), neural crest cells (numbered) showing the relative speed of neural crest compared to the neighboring tissue over a 2-hour window. Scale bar 20um. (G) Series of images from a typical time-lapse movie showing interaction between neural crest

(magenta) and mesodermal cells (green) over 8.5 hrs. Circles (neural crest). Squares and Triangle (mesodermal cells). Scale bar 20um.

Figure 3: Photoconverted region of tissue grows more in the dorsolateral direction than anterior-posterior. (A) Rectangular regions where Dendra2 was photoconverted from green to magenta in HH9 embryo and imaged again 8 hours later. Scale bar 100um. (B) Transverse views through embryo in (A) at the dashed yellow line highlighting the depth of photoconversion. Scale bar 50um. (C) Schematic of embryos indicating locations of photoconverted regions at HH9. Also, schematic of embryo with box showing the growth of the tissue in the medial-lateral (M-L) direction and compression in the anterior-posterior (A-P) direction but no change in the dorsal-ventral (D-V) direction. Colors of the side of the box coordinate with colors in graph. (D) Fold change in size of mesoderm photoconverted region in each direction. No change marked with horizontal dashed line. n = 13 embryos.

Figure 4: BrdU labeling of cells changes over time and throughout the tissue. (A) Averaged images of embryos from HH9, HH13 and HH15 with yellow nuclei if the Brdu/methyl green intensity is in the top 40% of cells. Scale bar 100um. (B) HH9 embryo with nuclei (red), neural crest (cyan) and BrdU (green). Second column of images shows area in dashed rectangle with spots segmented on the methyl green channel indicating location in the mesoderm (cyan) or ectoderm (magenta). Third column, HH15 labeled similarly. Scale bar 40um. (C) HH15 embryo with ba1 and ba2 streams marked mesodermal cells (cyan) and ectoderm (magenta). Scale bar 100um. (D) Area lateral to r3 studied marked with white spots. Scale bar 100um. (E) Schematic of distance measurement from the neural tube curving along the neural crest pathway. (F) Fraction of mesoderm cells in ba1, ba2, ectoderm overlaying the ba2 stream, or cells adjacent to r3 domains that are positive for BrdU label in stages HH9-HH15 with SEM bars. (G) Fraction of mesoderm cells BrdU-positive in 50um bins along the domain of r4 to the end of ba2. Dashed vertical lines represent the front of the neural crest stream. (H) Fraction of ectoderm cells BrdU-positive in 50um bins along the domain of r4 to the end of ba2.

Figure 5: Density of cells remains constant through r4 neural crest pathway. (A) Averaged images of embryos from HH9, HH13 and HH15 with orange nuclei indicating the densest 40% of cells. Scale bar 100um. (B) Transverse view of individual cells (mesoderm in cyan, ectoderm in magenta) in the r4 stream at HH9(above) and HH15 (below) shown by spheres of sizes representing distance to their nearest neighbor. Larger spheres have distant neighbors, small spheres have a close neighbor. (C) Nearest neighbor distance averaged for all mesoderm cells for ba1 and ba2 streams, ectoderm overlaying the ba2 stream, and area lateral to r3 with SEM bars. (D) Nearest neighbor distance between mesoderm neighbors in 50um bins along the domain of r4 to the end of ba2. (E) Nearest neighbor distance between ectoderm neighbors. (F) Schematic of neural crest migration, tissue density (orange) and proliferation (blue) changes over time

Figure 6: Modeling simulations of non-uniform tissue growth and the neural crest cell migratory pattern. (A) Schematics of tissue growth profiles. Darker color indicates a higher growth rate. The growth rate is doubled for half of the domain in models D and P. As the cells migrate into the domain, they are advected at different rates and also contribute individual velocity to reach the end of the domain. Right, example of final distribution of cells (green) on a domain with chemoattractant concentration (red/black color bar). Model M combines proximal (P) and distal (D) growth profiles such that for less than 18 hours embryonic time the domain follows model D and from time greater than 18 hours the model follows growth profile P, with input cell velocity of 42um/min. (B) Left: Length of the simulated neural crest cell migratory stream at 24hrs using different input cell speeds (42,45,48,51 um/hr). Right: neural crest speed throughout the domain with different input speeds (42,48,51 um/hr) as cells are also advected with the domain growth.

Figure 7. Physical ablation of premigratory neural crest cells or chemical inhibition of mesoderm growth show affects to both the neural crest cell migratory pattern and tissue growth. Representative r4 neural crest cell migratory stream 24 hrs post bi-lateral ablation of premigratory neural crest cells: (A) control (left) and ablated (right) stained with methyl green for all nuclei (red), HNK-1 for neural crest

(cyan) and BrdU for proliferation (green). Scale bar 100um. The simulated control and ablation (modeled by reduction in number and delay of cells entering the domain) of premigratory neural crest cells (far right panels) scenarios with growth profile (M) as mentioned in Fig. 6. (B) Length of domain and neural crest stream and the ratio for control and ablated embryos, n=10 for ablated and 12 for control. Far right bars (green/red) are the ratio of neural crest stream to domain length in simulated neural crest ablations. (C) Fraction of non-neural crest cells in domain BrdU positive for control and ablated embryos. Vertical line indicates average length of neural crest stream. (D) Schematic of VEGF IHC and the potential increase in VEGF concentration post neural crest ablation. Below, images of mesodermal cells in culture with or without exposure to VEGF for 16 hrs labeled with Hoescht for nuclei (magenta), HNK-1 for neural crest (cyan) and BrdU (green). Scale bar 100um. (E) Fraction of mesoderm cells in vitro that are BrdU-positive with (n=5) or without VEGF (n=8). (F) Schematic and representative embryo injected with a cocktail of aphidicolin, hydroxyurea and DiD (green) after 8 hrs incubation. IHC performed with methyl green (red) and HNK-1 (cyan). Scale bar is 100um. The simulated control and domain growth inhibition panels are shown on the far right after 8 hrs of simulation time to correspond to the experimental data. (G) Length of domain and neural crest stream and ratio of 8 treated and 8 control embryos. Far right bars (red/green) are the ratio of neural crest stream length to domain length in simulated chemical inhibition of domain growth.

Figure 8: In vivo time-lapse imaging of head mesodermal cell behaviors pre neural crest emergence. (A) Transverse view of r4 area over 3.5 hours in a time-lapse. Neural crest (magenta, leader marked with star) have just emerged from the neural tube while the surface ectoderm is changing shape. Scale bar 50um. (B) Image of embryo at beginning of time-lapse with center of whirling motion and approximate size of circle marked. Scale bar 100um. (C) Displacement of mesodermal and ectoderm cells (white arrows) over eight hours of imaging. (D) Color-coded time projected over a two-hour window with purple being time zero and yellow two hours later. The circular rotation of cells can be seen across from the r3/r4 boundary. Comparison of Speed (E) and Directionality (F) of mesodermal cells before and after the neural crest emerge from r4.

1
2
3
4 **Supplementary Figure 1. Mesoderm explants rarely contain neural crest cells.** (A)

5
6 An example neural tube explant labeled with Hoechst and HNK1 by IHC with many
7 labeled neural crest migrating away from the neural tube. (B) A mesoderm explant
8 labeled similarly with only a few neural crest.
9

10
11
12 **Supplementary Figure 2. Speed and directionality of tracked mesoderm cells with**
13 **spatial location.** All tracked cells displayed at their first tracked location colored by
14 speed (A) and directionality (B) in rainbow color palette. Other than the cells adjacent to
15 r3 being slower, there is not a clear correlation of spatial location and either of these
16 parameters. Asterisk indicates midline position of rhombomere 4 and circle represents
17 approximate area of future otic vesicle.
18
19
20
21
22

23
24 **Supplementary Figure 3. Proliferation of mesoderm cells in between r1 and ba1.**

25
26 Fraction of cells BrdU positive in 50um bins along the domain between r1 to the end of
27 ba1 (domain highlighted in Figure 4C). n = 2 for HH9, n=3 for HH11, n=5 for HH13, and
28 n=4 for HH15.
29
30
31

32 **Supplementary Figure 4. Density measurement flaws using inaccurate volume**
33 **segmentation.** (A) Example images of HH11 and HH15 embryos with mesoderm
34 (cyan) and ectoderm (magenta) nuclei labeled. Scale bar 50um (B) Estimated volume
35 using nuclei broken into 50um along the neural crest migratory pathway. (C) Density
36 measurements (number of cells/volume) for all embryos both mesoderm and ectoderm.
37 Large SEM bars indicate high variation between embryos for this type of measurement.
38 Though the trends are similar, measuring the nearest neighbor distance results in a less
39 variable measurement.
40
41
42
43
44
45
46
47

48 **Supplementary Movie 1. Lateral mesoderm cells in culture migrates dynamically.**

49
50 Hoechst labeled explanted lateral mesoderm from HH10 chick embryo imaged in 5-
51 minute intervals for approximately 16 hours.
52
53

54 **Supplementary Movie 2. Neural tube culture illustrating the dynamically migrating**
55 **neural crest.** Hoechst labeled neural tube explant imaged in 5-minute intervals for
56 approximately 16 hours. Many neural crest can be seen exiting the neural tube and
57 exploring the dish.
58
59
60
61
62
63
64
65

1
2
3
4 **Supplementary Movie 3. Neural crest cells interact with mesoderm cells in vitro.**

5
6 Hoechst labeled neural tube explant and mesoderm explant imaged in 5-minute
7
8 intervals for approximately 16 hours.
9

10
11 **Supplementary Movie 4. Tracked neural crest and mesoderm cells in vitro.**

12 Hoescht labeled neural tube explant and mesoderm explant zoomed in near interaction
13 site with some cells' tracks shown in green and magenta. Cells are labeled identically
14 so hand-drawn tracks were made during periods where cells can be distinguished. If a
15 cell moves to a highly dense area, the track is stopped.
16
17
18
19

20
21 **Supplementary Movie 5. Mesoderm adheres to ectoderm when cultured together.**

22 Hoechst labeled and mesoderm and surface ectoderm explant imaged in 5-minute
23
24 intervals for approximately 16 hours
25

26
27 **Supplementary Movie 6. neural crest bulldoze through the mesoderm displacing**

28 **cells.** Dorsal view of transgenic quail embryo (green) with DiD neural crest (magenta).

29 Three mesoderm cells are highlighted in white and some of the neural crest they
30 interact with are highlighted in magenta. The mesoderm cells can be seen to passed by
31 the neural crest and diverted posteriorly (1, squares), become more directed and seem
32 to be pushed (2, circles), or move far posterior to its original location and eventually
33 passed by the neural crest stream (3, triangle).
34
35
36
37
38
39

40
41 **Supplementary Movie 7. Whirling motion of ectoderm and mesoderm can be**

42 **observed lateral to r3.** Dorsal view of transgenic quail (green) with DiD labeled neural
43 tube and migratory neural crest cells (magenta). Before the neural crest emerge from
44 the r4 axial level a counterclockwise rotation of cells can be observed at r3. Confocal z-
45 stack images taken in 7-minute intervals for several hours.
46
47
48
49

50
51 **Supplementary Movie 8. Neural crest migrate much faster than the ectoderm**

52 **sliding under the tissue.** Transverse (top) and Dorsal (bottom) views of transgenic
53 embryo (green) with DiD labeled neural tube and neural crest (magenta) of HH12 stage
54 quail embryo. The cyan marked ectoderm cells move very little compared to the neural
55 crest marked in yellow that slide beneath. Images taken in 4.5-minute intervals for
56
57
58
59
60
61
62
63
64
65 several hours.

Supplementary Movie 9. Gross morphological changes during neural crest migration at the r4 axial level. Transverse view of the r4 axial level of a whole transgenic quail embryo culture (green) with DiD labeled neural crest and neural tube (magenta). The tissue bends and grows ventrally while cells stream laterally. Confocal z-stack images taken in 7-minute intervals for several hours.

Figure 1

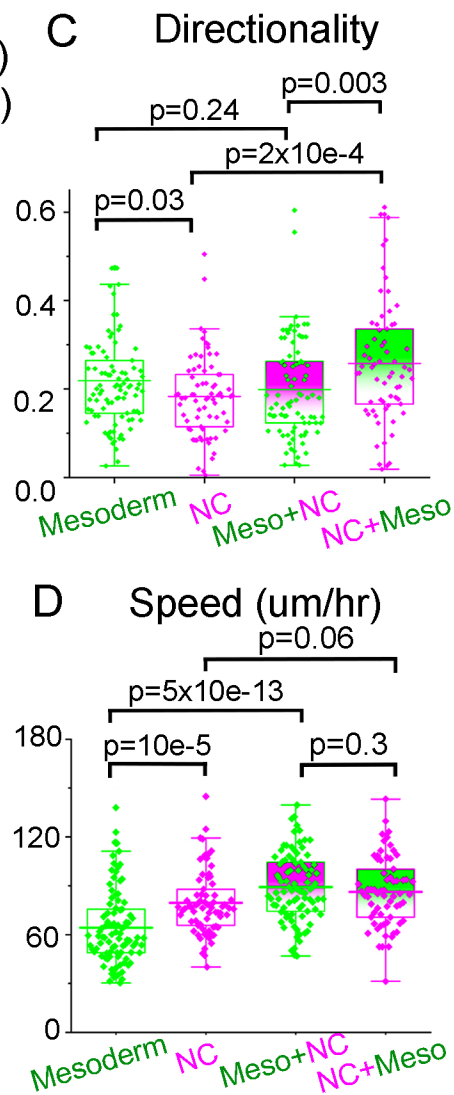
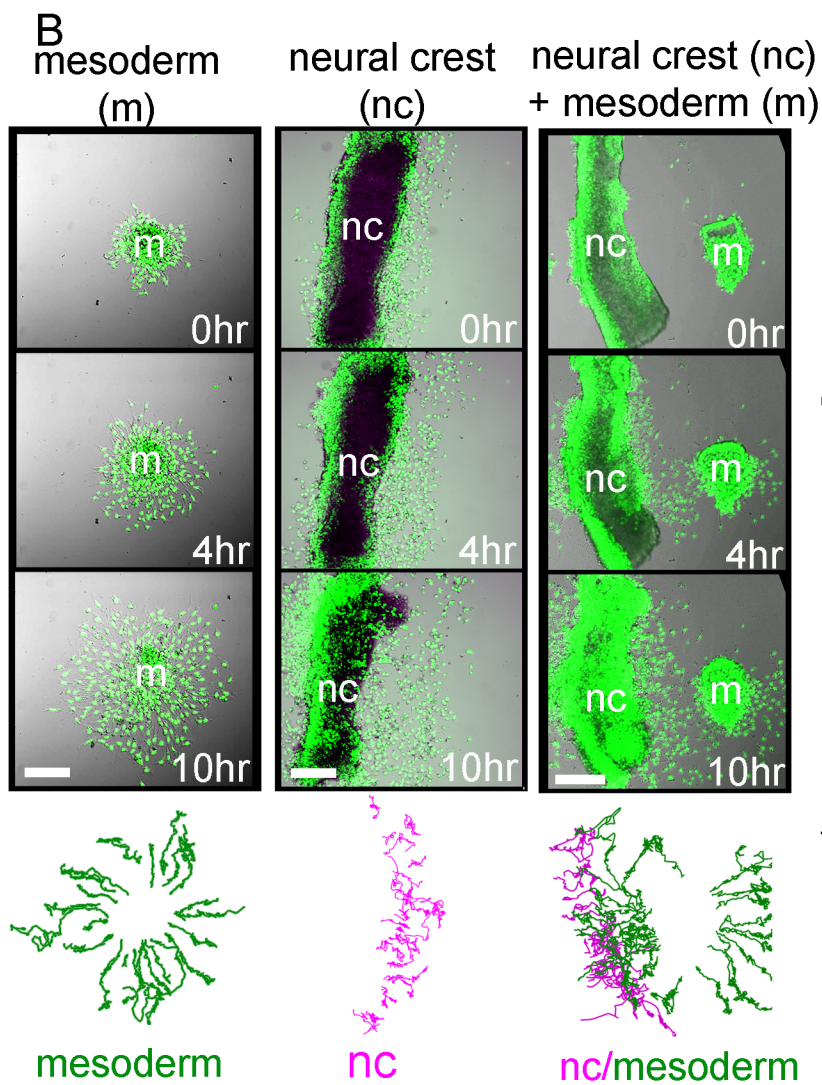
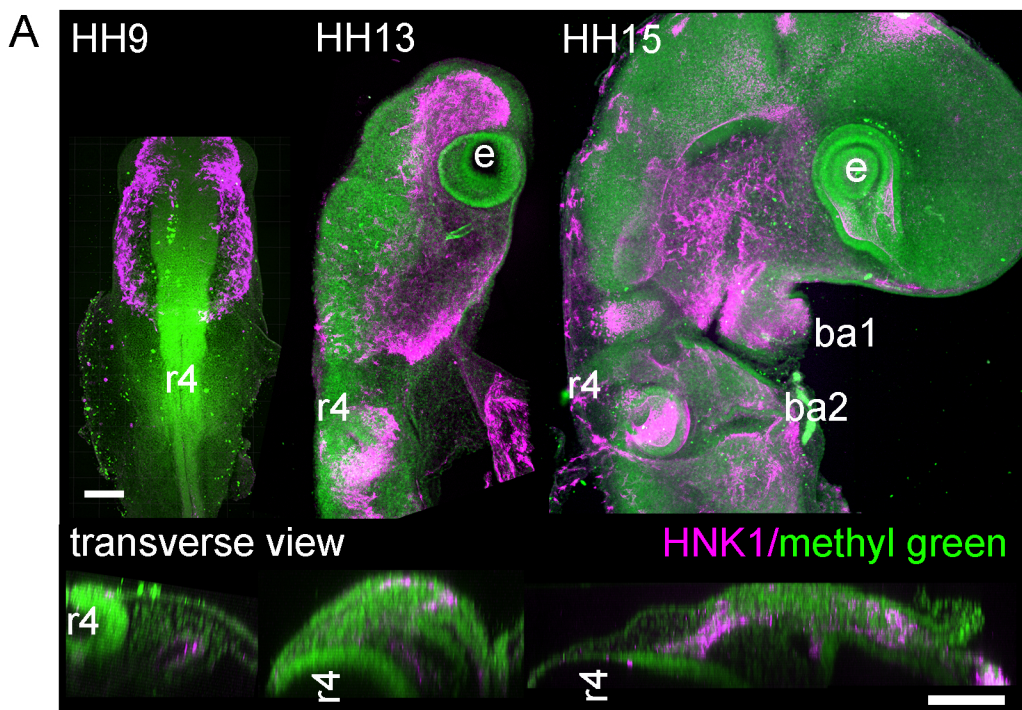


Figure 2

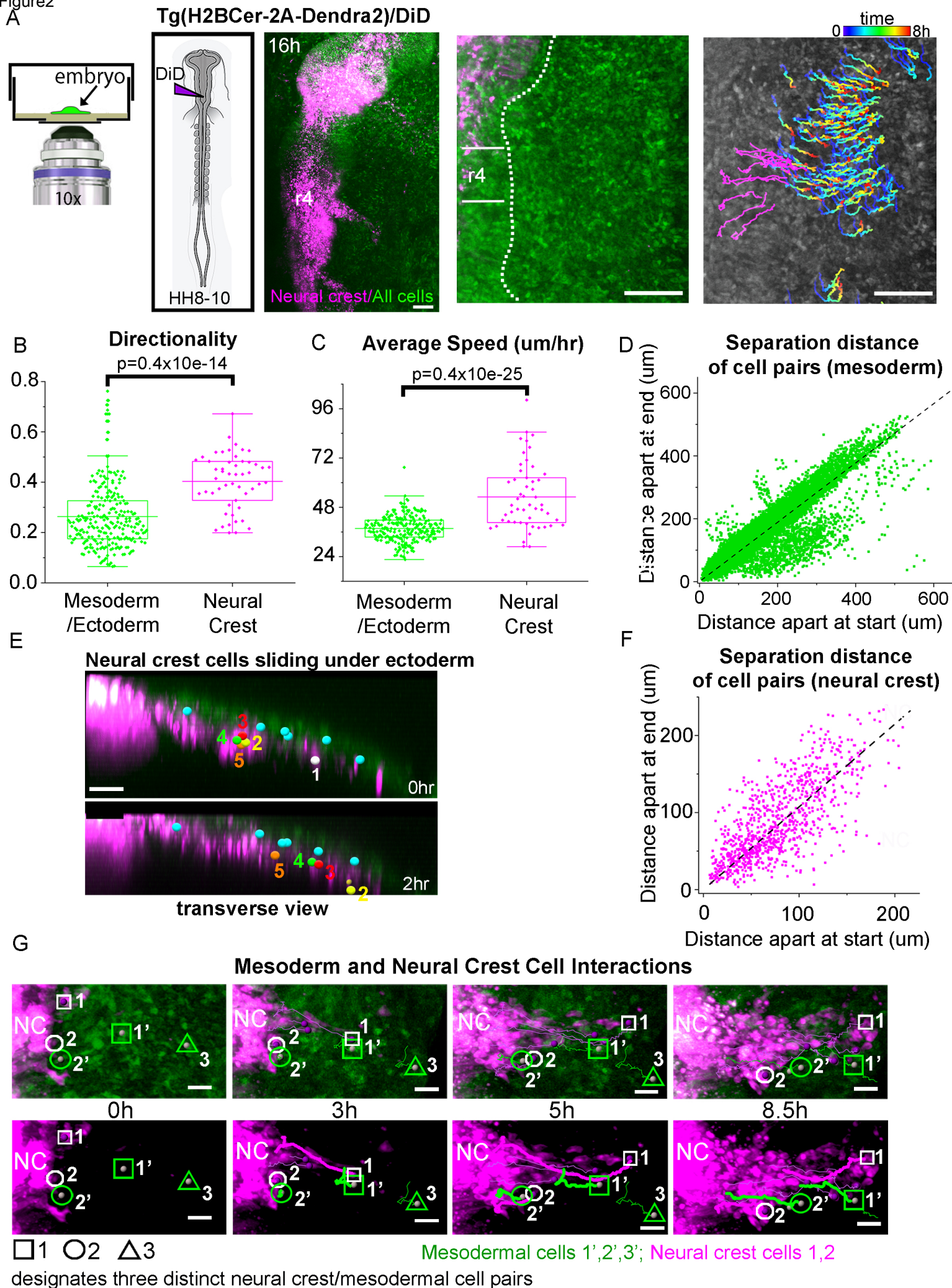
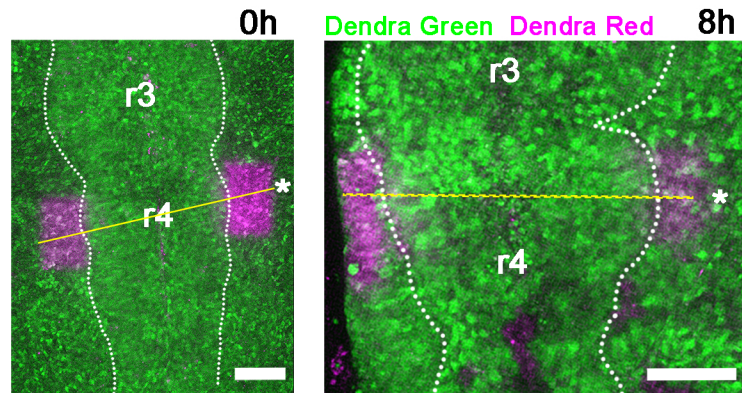


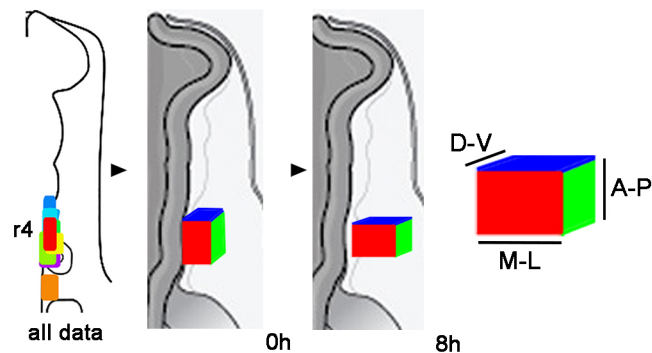
Figure 3

A Tissue shape changes using photoconversion

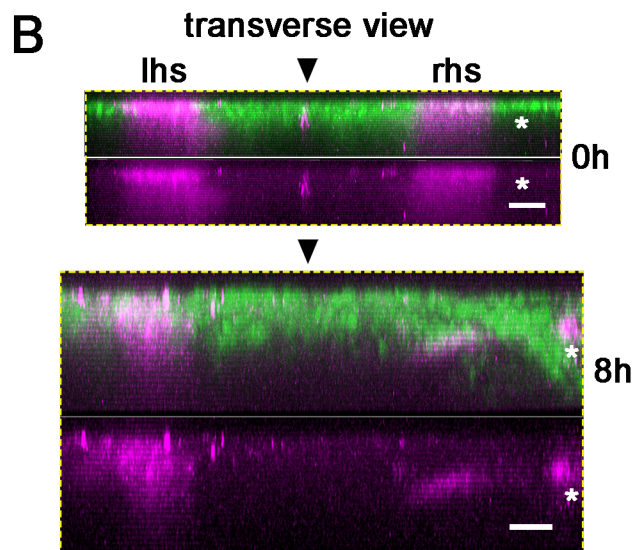


Tg(hUBC: H2BCerulean-2A-Dendra2)

C Photoconversion Region and Measurement



B



D

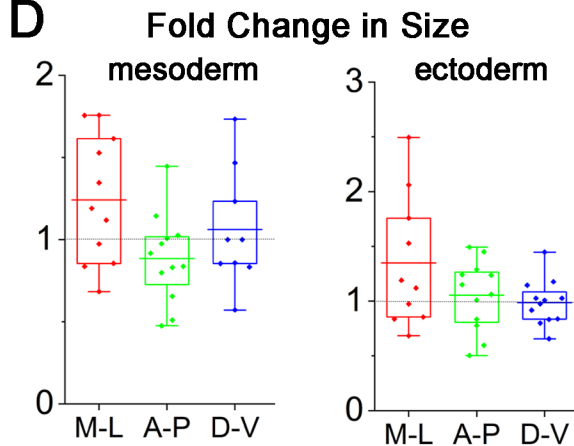
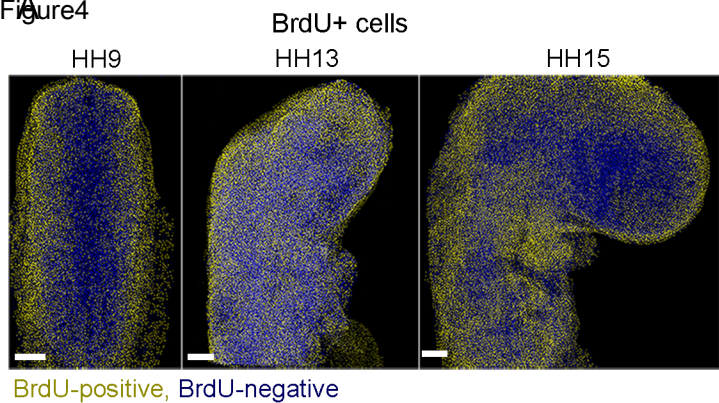
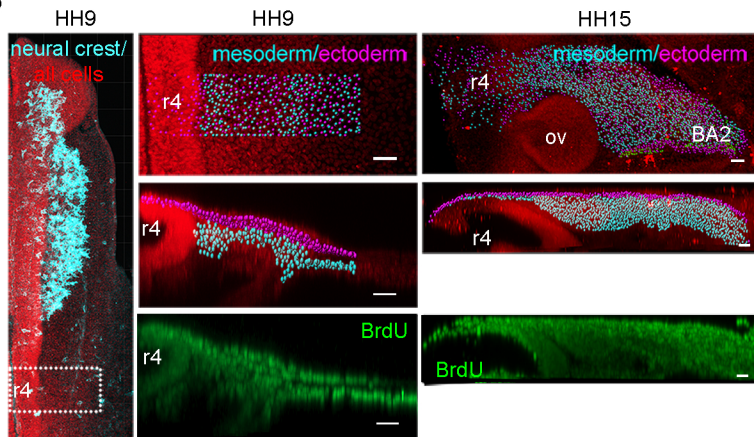
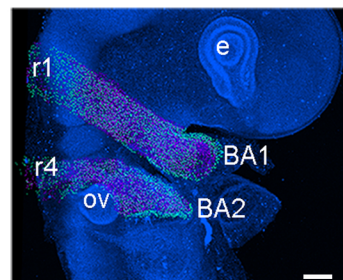
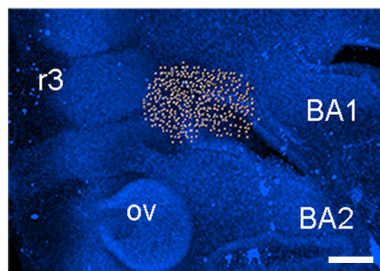
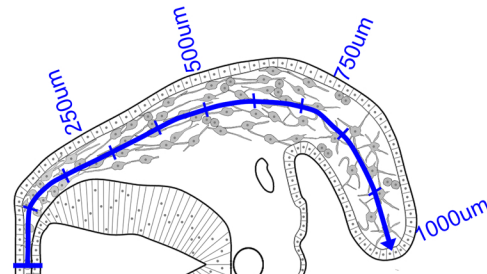


Figure 4**B****C****D****E schematic of distance measurements****F Fraction of Cells BrdU-positive**

BA2 stream BA1 stream
Ectoderm r3 near

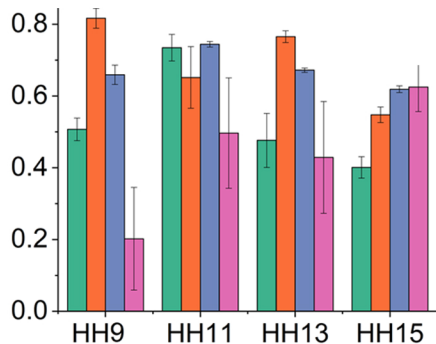
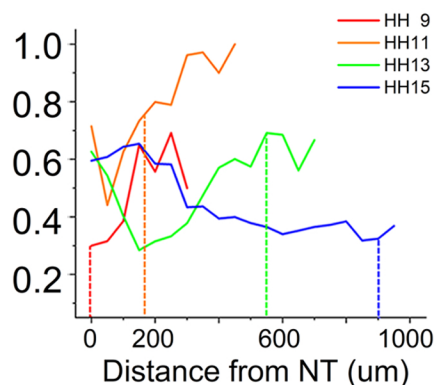
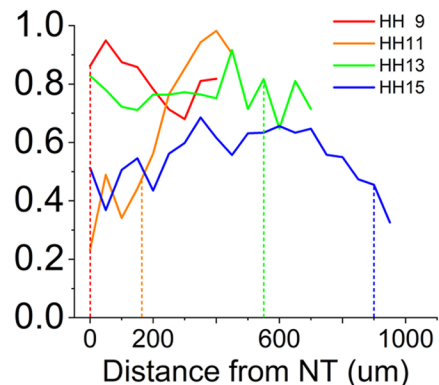
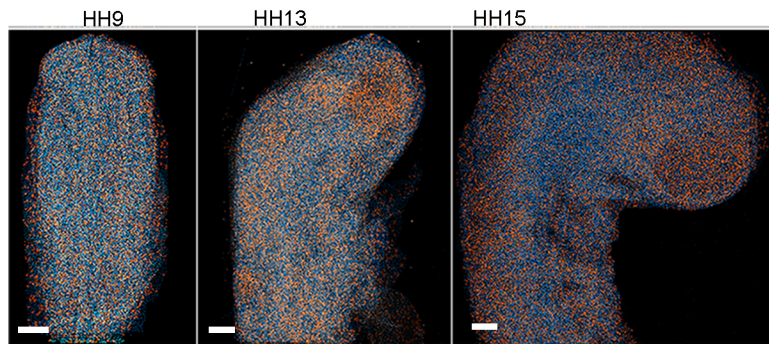
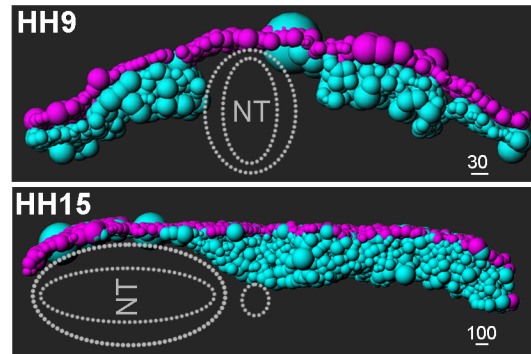
**G****Mesoderm Fraction Cells BrdU+****H****Ectoderm Fraction Cells BrdU+**

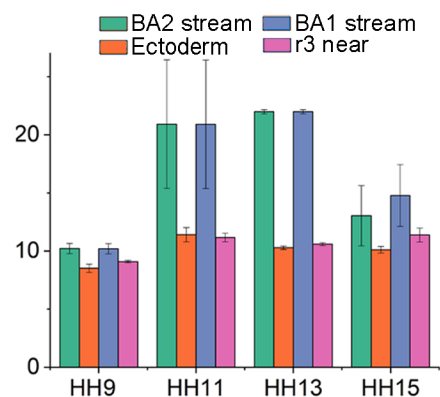
Figure 5 **A** Nearest Neighbor



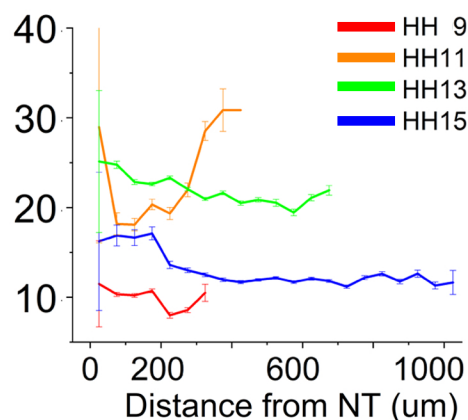
B Nearest Neighbor Calculation



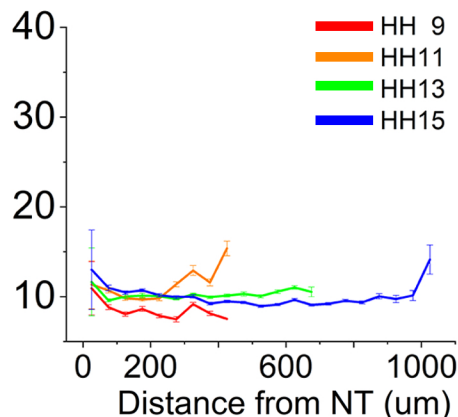
C Nearest Neighbor (um)



D Nearest Neighbor Mesoderm (um)



E Nearest Neighbor Ectoderm (um)



F Cell BrdU and nearest neighbor schematic

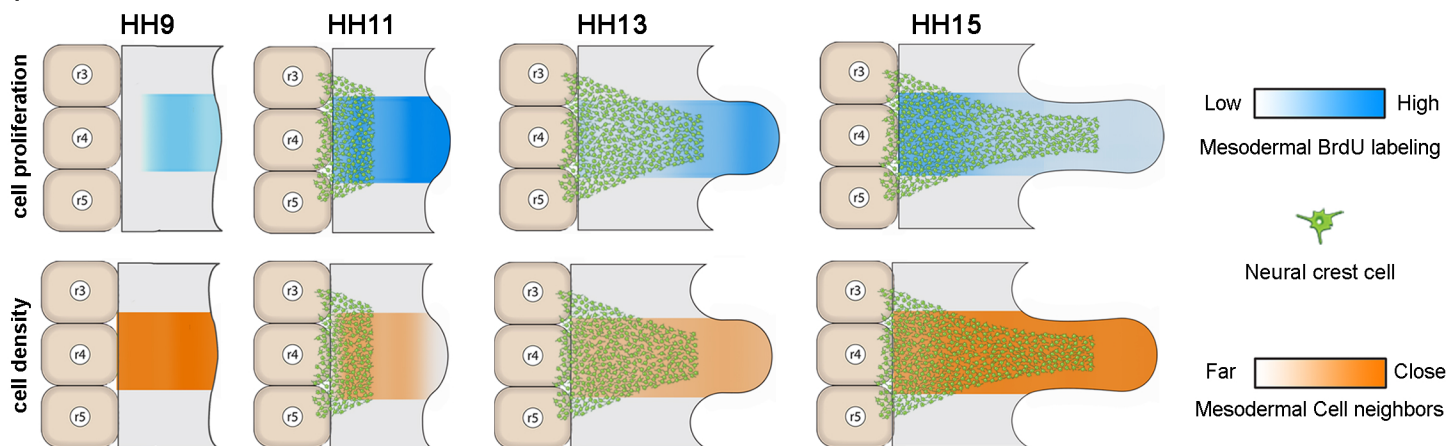
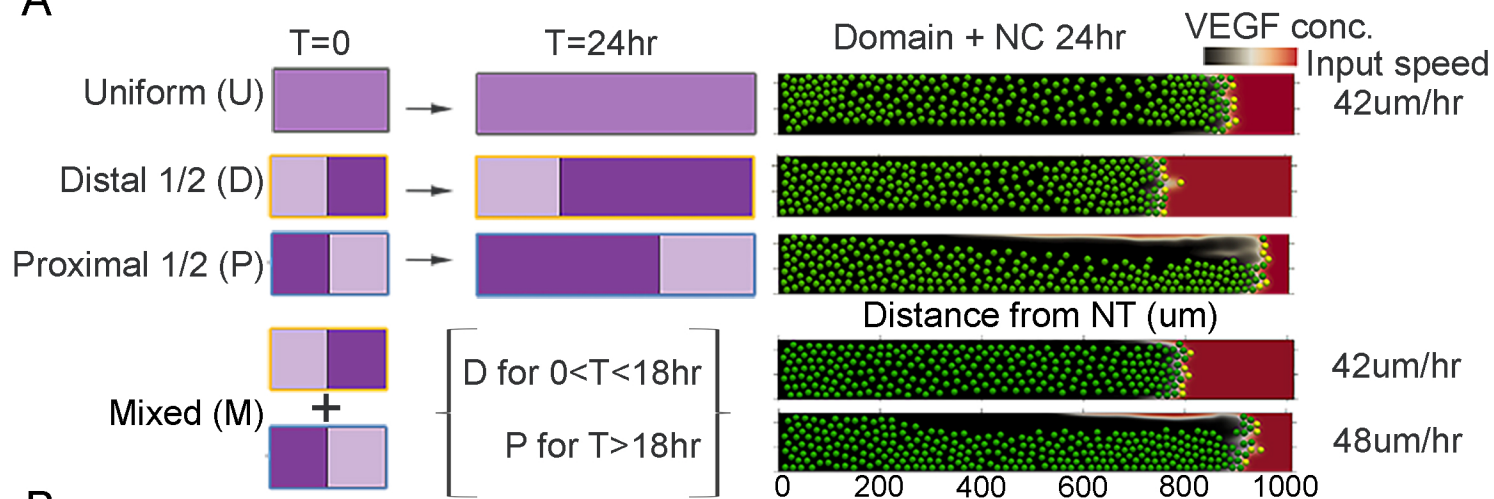


Figure 6

A



B

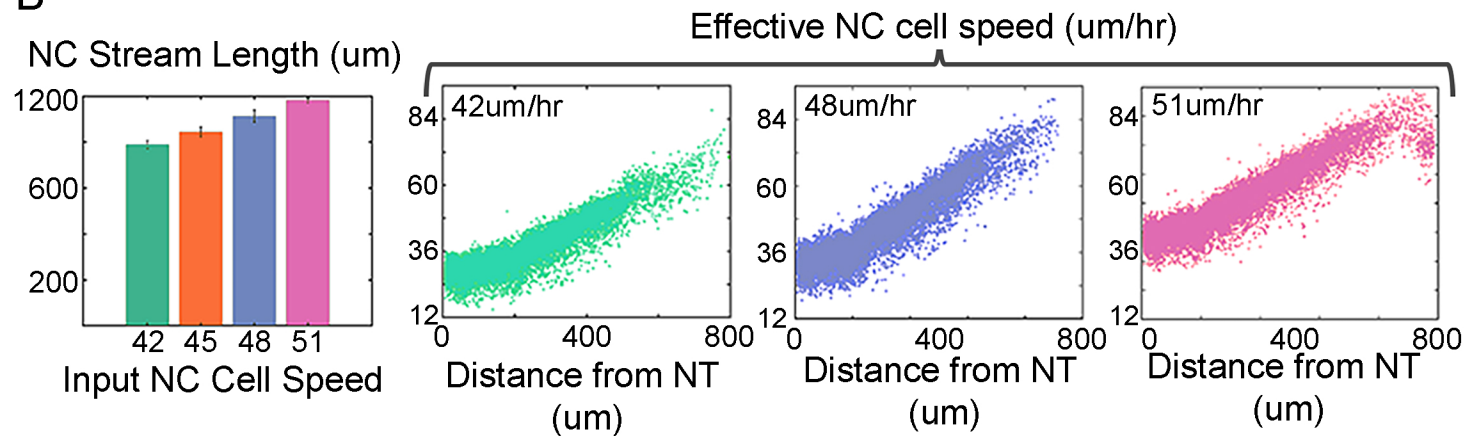
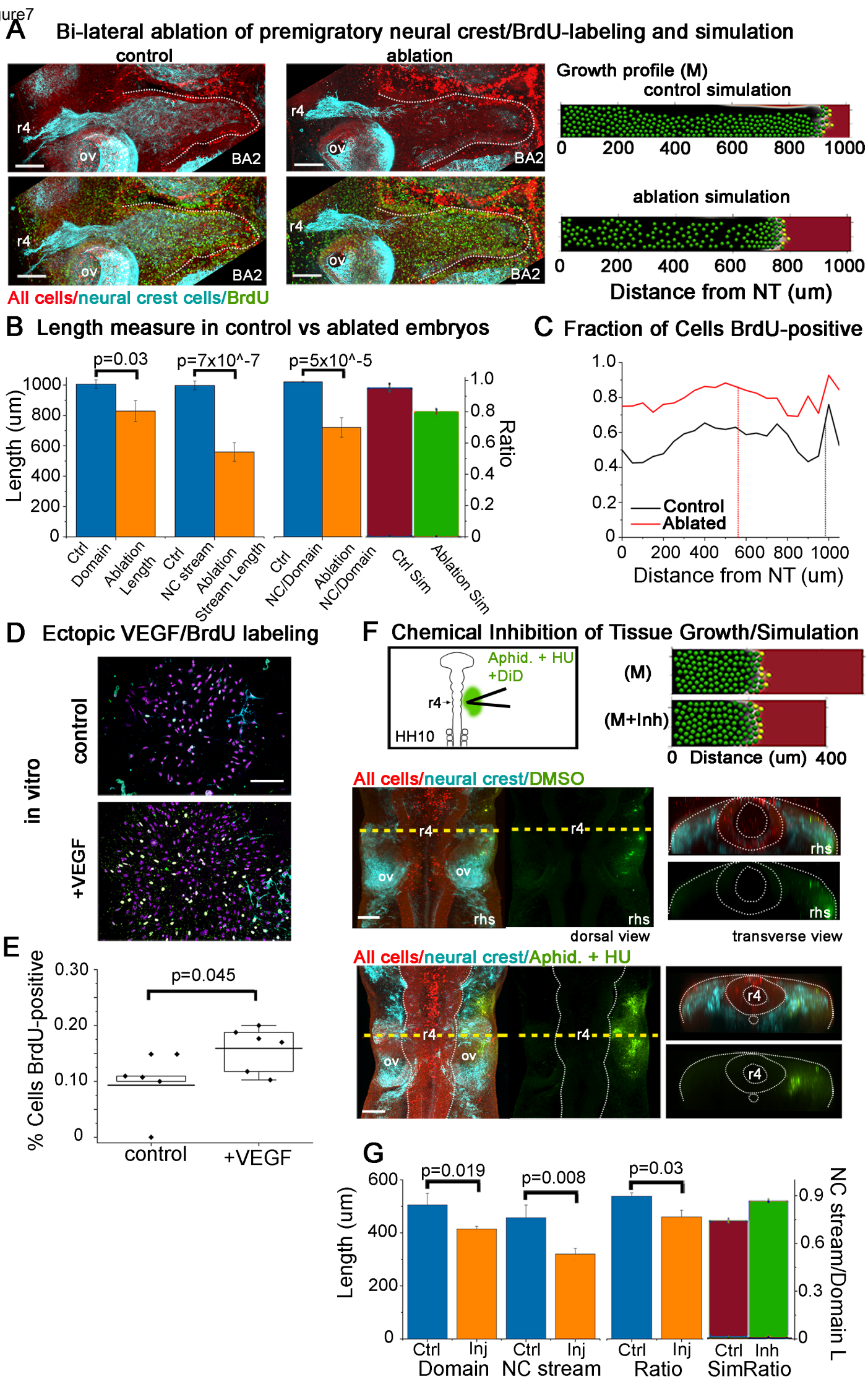
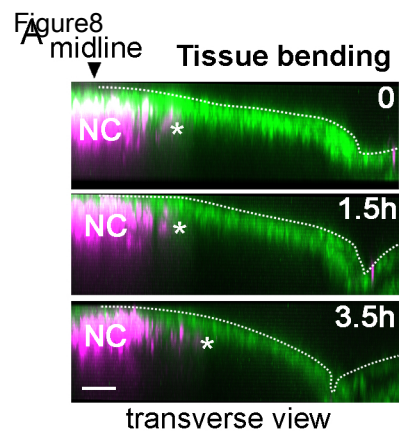
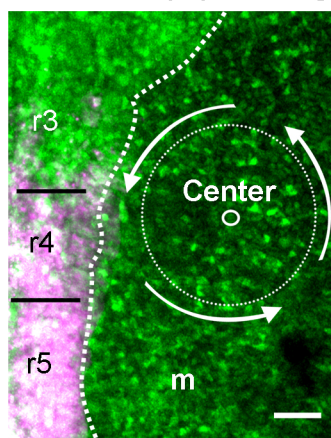


Figure 7

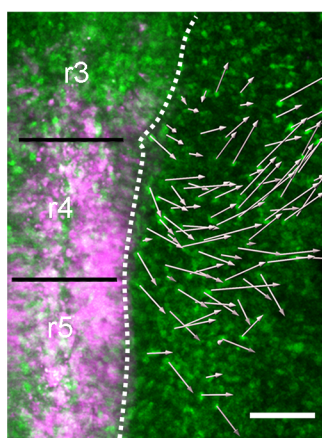




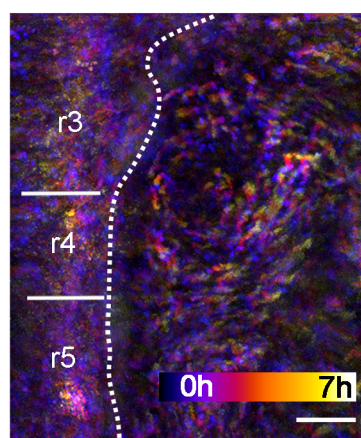
B Mesoderm (m) swirling



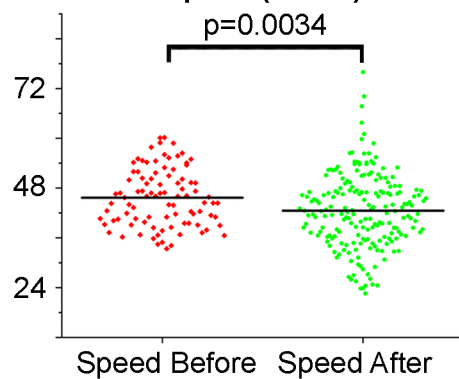
C Vector analysis



D Particle motions



E Speed (um/hr)



F Directionality

